ISET Journal of Earthquake Technology, Paper No. 523, Vol. 50, No. 1, March 2013, pp. 1–26

EARTHQUAKE RESPONSE OF A THREE-SPAN BRIDGE, WITH MID-SPAN SUPPORTED BY PINS, TO NEAR-FIELD PULSE AND PERMANENT-DISPLACEMENT STEP

Reza S. Jalali[*], Masoumeh Bahari Jokandan[*] and Mihailo D. Trifunac[**]

[*]Department of Civil Engineering
University of Guilan, P.O. Box 3756, Rasht, Iran
[**]Department of Civil Engineering
University of Southern California, Los Angeles, CA 90089, U.S.A.

ABSTRACT

Wave passage and differential motions of long structures can lead to excessive demands in the near field of strong earthquakes. For long and stiff structures these demands are dominated by pseudo-static deformations resulting from differential ground motions. In our previous work we confirmed that replacing continuous bridge girder with multiple short segments, interconnected by structural joints, reduces pseudo-static forces in the piers. In this paper these reductions are further examined for a three-span bridge, with the mid-span supported by pins. It is shown that the placement of pins in the mid-span, rather than over the piers, results in only minor differences in the forces and drifts in the bridge. Shear forces in the joint keys, as well as the drifts of piers, for the out-of-plane response are again reduced in the high-frequency band in the bridge that is made flexible by the placement of joints in the middle span.

KEYWORDS: Spatial Seismic Effects, Ground Rotations, Structural Torsion, Reduction of Shear Forces in Joint Keys, Reduction of Pseudo-Static Actions

INTRODUCTION

For large and long structures, the effects of differential earthquake ground motions become significant and should be considered in the design (Bogdanoff et al., 1965; Okubo et al., 1983; Zembaty and Krenk, 1993, 1994). Contributions caused by the differential ground motions to the total response have been studied for beams (Harichandran and Wang, 1988, 1990; Zerva, 1991), bridges (Kashefi and Trifunac, 1986; Perotti, 1990; Hyun et al., 1992), simple models of three-dimensional structures (Hao, 1991), long buildings (Todorovska and Lee, 1989; Todorovska and Trifunac, 1989, 1990a, 1990b), and dams (Kojić and Trifunac, 1988, 1991a, 1991b).

Extensions and generalizations of the classical response-spectrum method, which are based on the Taylor-series approximations of long-wave ground motions, cease to be valid for short-wave excitations. Such extensions have been described in the studies involving differential strong motions (Jalali and Trifunac, 2009, 2011; Trifunac and Todorovska, 1997a; Trifunac and Gicev, 2006) and strength-reduction factors (Jalali and Trifunac, 2007, 2008; Jalali et al., 2007). Hao (1998) studied the required seating length to avoid the unseating and pounding of the adjacent bridge decks. Zanardo et al. (2002) confirmed the significance of spatially non-uniform ground motions, and Chouw and Hao (2003, 2004, 2005) showed that neglecting the soil-structure interaction (SSI) effects and ground-motion spatial variations will result in an inaccurate prediction of the pounding response of bridge girders.

The purpose of this paper is to extend the results of Jalali et al. (2012), who analyzed the seismic response of a simple, symmetric model of a three-span, simply supported bridge (see Figure 1(a)) to the fault-parallel and fault-normal displacements near faults. In this paper we study the same bridge, but move the pins of the central span away from the piers, as shown in Figure 1(b). To emphasize only the consequences of differential, but propagating and transient fault-normal pulses and fault-parallel displacements, it will be assumed again that soil-structure interaction can be neglected. The impulsive ground motion near an earthquake fault, and in particular the amplitude and period of the velocity pulses there, can have a significant effect on the performance of structures (Hall et al., 1995; Mylonakis and Reinhorn, 2001; Dicleli, 2008; Fenves and Ellery, 1998; Jonsson et al., 2010; Trifunac and Todorovska, 1994; Goel and Chopra, 2008). The large pulses in acceleration, velocity and displacement time histories

can also propagate to considerable distances from the fault and maintain their amplitudes and polarity over distances as large as tens of kilometres (Todorovska and Trifunac, 1997).

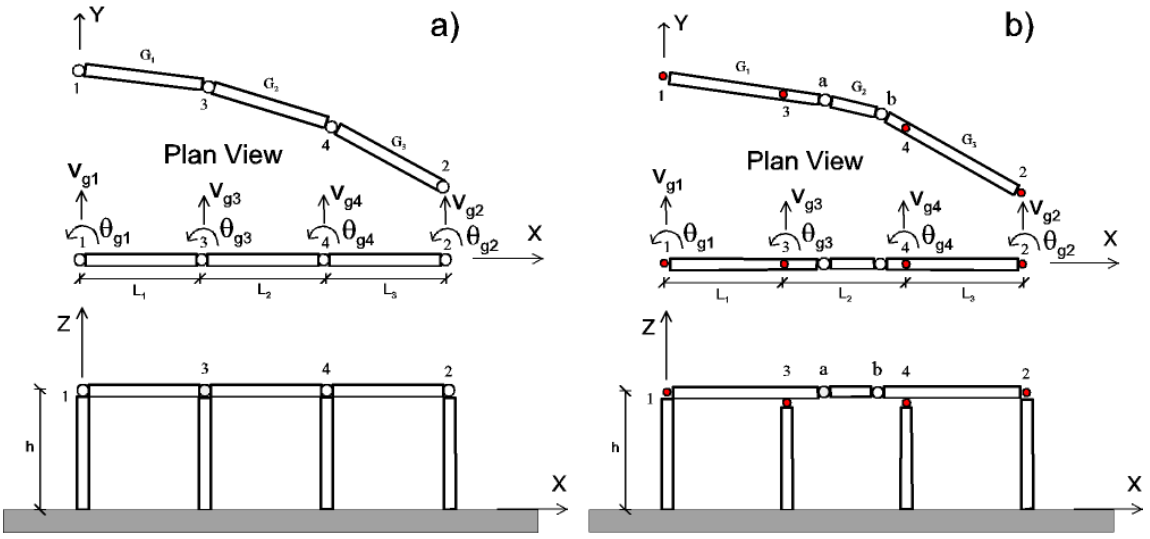

Fig. 1 Plan view (top) and side view (bottom) of the schematic representation of a bridge (a) with pins over the columns (from Jalali et al., 2012) and (b) with pins in the central span (as studied in this paper)

This study aims to illustrate qualitatively the dynamic consequences of wave-passage effects on long, bridge-like structures for idealized, near-fault, strong-motion pulses, to show the advantages of the flexible, long structures, which can follow the deformations imposed by the propagating waves, and to show that the placement of the joints supporting the central span does not alter the overall trends in the response. A sensitivity analysis of the dependence of the response on many other governing variables and of the range of their possible values is beyond the scope of this paper. In this paper we consider only the wave-passage effects. We do not consider coherency loss, which is poorly understood and difficult to model in the near field.

DYNAMIC MODEL

The model we consider is a symmetric three-span bridge, with middle hinges at distances a and b from the central columns (see Figure 1(b)), consisting of three rigid decks with masses m_1, m_2, m_3, polar mass moments of inertia J_1, J_2, J_3, and lengths L_1, L_2, L_3, which are supported by four axially-rigid, massless piers connected at the top to the decks and at the bottom to the ground by circular rotational and torsional springs. The rotational and torsional springs represent the bending and torsional stiffnesses of the piers. It is assumed that there is no soil-structure interaction so that the points on the ground surface where the piers are supported move as in the free-field strong motion. At the middle hinges the rigid decks are interconnected by rigid shear keys to prevent an out-of-plane relative displacement and unseating. The massless piers are connected to the ground and to the rigid deck by linear circular rotational and torsional dashpots to provide the prescribed fraction of critical damping. The rotation of the piers is assumed to be small enough so that the interaction between the in-plane and out-of-plane motions of the rigid decks may be neglected. The bridge is acted upon by the acceleration due to gravity, g and is excited by the differential out-of-plane and torsional ground motions. The bridge model considered and its governing equations are described in Appendix I.

NEAR-FAULT GROUND MOTION

To describe the ground motions near faults we consider the fault-normal pulse d_F and the fault-parallel permanent displacement d_N and select their amplitudes and duration to be consistent with what is known about the nature of these motions. Figure A.5 in Appendix II shows schematically a fault and these two (characteristic) motions, which describe the monotonic growth of the displacement toward the permanent static offset and a pulse that is assumed here to be perpendicular to the fault and associated with the failure of a nearby asperity or passage of dislocation under or past the observation point. Further discussion and motivation for selecting these simple (strong-motion) displacement functions can be found in the previous work of the authors (Jalali and Trifunac, 2007, 2008, 2009).

The motions d_N and d_F have large values of initial velocity. This parameter is proportional to the stress drop on the fault, and even in the presence of nonlinear site response, it can be in the range of hundreds of cm/s (Trifunac, 1998, 2009).

STRUCTURAL RESPONSE

As in Jalali et al. (2012), it is assumed that $L_1 = L_2 = L_3 = L$ = 30 m and, for different phase velocities, different values of time delay τ are selected (τ = 0.03, 0.05, 0.1, 0.2, 0.3 s). The height of the bridge is h = 6 m and the torsional stiffness of piers is neglected (i.e., K_{TC} = 0). The contribution of all the modes of the bridge is included in all analyses and the damping ratio of the first mode is supposed to be ζ_1 = 0.02. The period of the first mode of the bridge, T_1, is assumed to vary between 0.1 and 1.5 s and all the results are shown versus T_1. In the nonlinear analyses, the material behaviour of piers in bending is assumed to be elasto-plastic and the yielding limit of the rotational springs of piers is supposed to be ϕ_y = 0.005 and 0.01.

In this paper only the action of the out-of-plane component (along the Y-axis; see Figures 1(a) and 1(b)) of the near-fault ground motion, v_{g_i}, is considered at the base of the piers for the earthquake magnitude M = 4 to 7, but the effects of foundation-soil interaction are neglected. It is assumed that the bridge is near a fault and that the longitudinal axis of the bridge (i.e., the X-axis) coincides with the radial direction (along the r-axis) of the propagation of waves from the earthquake source, so that the absolute displacements of the bases of piers because of the wave passage are different. It is further assumed that the ground motion can be described approximately by a linear-wave motion. Thus, the nonlinear soil strains and cracks in the soil, which accompany violent, strong ground motion in the near field, will not be considered here (Trifunac and Todorovska, 1996, 1997a, 1997b, 1997c; Trifunac et al., 1996). By considering the wave propagation from left to right in Figure 1(b), it is assumed that the excitations at all the four piers have the same amplitude but differ in terms of phases. The phase difference (or the time delay τ) between the four ground motions depends on the distance between the piers and the horizontal phase velocity of the incident waves. As shown in Figure 1(b), the system is excited by differential out-of-plane ground motions, v_{g_i}, i = 1, 2, 3, 4 at the four bases, such that

$$v_{g_2}(t) = v_{g_1}(t-\tau) \tag{1a}$$

$$v_{g_3}(t) = v_{g_1}(t-\tau/3) \tag{1b}$$

$$v_{g_4}(t) = v_{g_1}(t-2\tau/3) \tag{1c}$$

$$\tau = 3L/C_x \tag{1d}$$

where C_x is the horizontal phase velocity of the incident waves. The functional form of $v_{g_i}(t)$ is defined by Equations (A.23) and (A.24) (see Appendix II) for the fault-normal pulse and fault-parallel displacements, respectively. For body waves, C_x depends on the shear-wave velocity β in the half space and on the incident angle γ. For surface waves, C_x depends on the dispersion characteristics of the

medium (it may be noted that $C_x(\omega)$ is different for each of the surface-wave modes; Todorovska et al., 2013). For plane waves, the value of C_x varies between β and infinity (i.e., $\beta < C_x < \infty$), and in this paper, it will be assumed to vary between 300 m/s and infinity (i.e., $300 < C_x < \infty$).

For each specific design of a bridge, there will be some torsional resistance between the deck ends and the piers. In Jalali et al. (2012), the torsional resistance between the middle piers and the deck ends at the two sides was modeled by a torsional spring with the stiffness $0.5K_{TC}$, and the torsional resistance between the end piers and the deck ends was modeled by torsional springs with the stiffness K_{TC}, where K_{TC} is the torsional stiffness of the piers (see Figure A.2(a)). The ratio of torsional to bending stiffness for each pier, K_{TC}/K_{ϕ}, depends on the number of columns at each pier, the width of the bridge and the piers, the distance between the columns of each pier, and the cross-section and height of the columns of each pier and their material properties (see Figure A.2(b)). The ratio K_{TC}/K_{ϕ} is expected to vary between 0.1 and 2.0 (Jalali et al., 2012).

RESULTS

Based on the above formulation (see Equation (A.10)), we analyzed the response of a three-span bridge with middle shear keys and different main periods, when it is excited by the fault-parallel and fault-normal displacements for different earthquake magnitudes and time lags of wave arrival to the base of the columns. The linear response of the bridge is shown in Figures 2–4 and the nonlinear response of the system is presented in Figures 5–8.

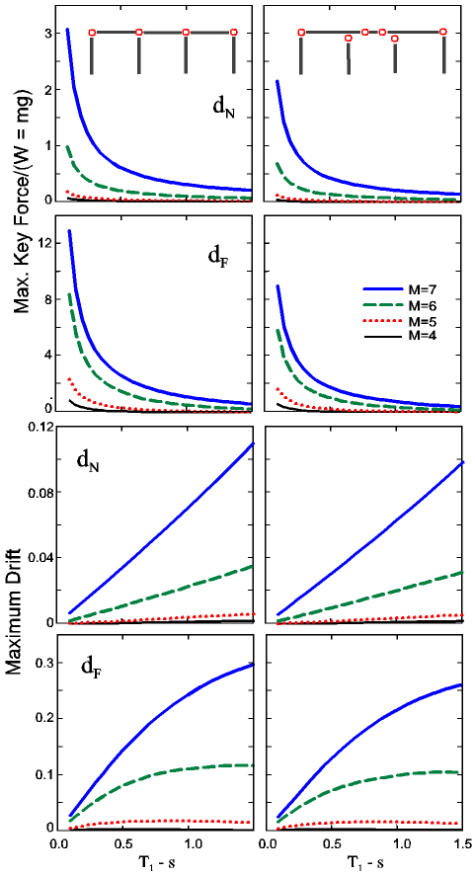

Fig. 2 Maximum linear-shear-key forces (top two levels) and drifts (bottom two levels) in the piers versus fundamental period T_1 for fault-parallel displacement d_N and fault-normal pulse d_F, magnitudes M = 4, 5, 6, 7, τ = 0 and K_{TC} = 0, for the bridge models with pins over the columns (left) and in the central span (right)

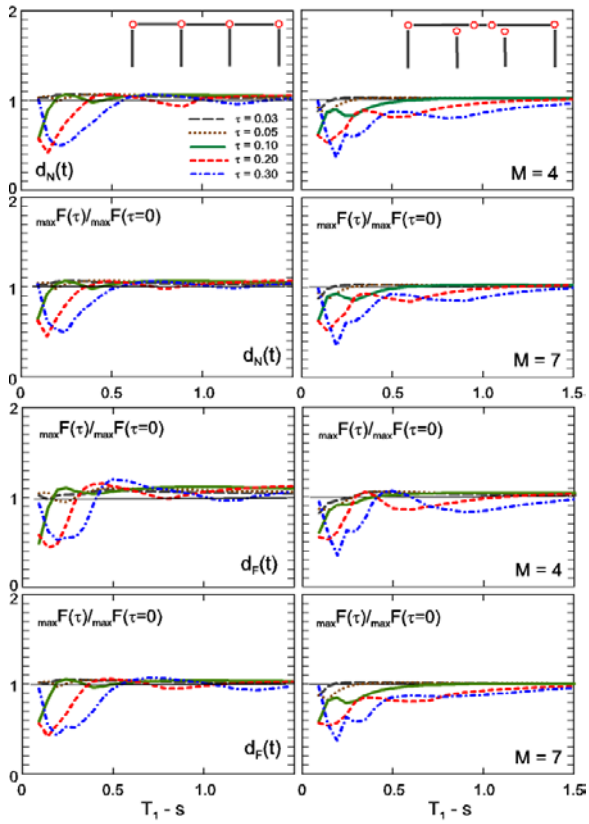

Fig. 3 Wave-passage effects on the magnification factors of maximum linear-shear-key forces versus system fundamental period T_1 for time lag τ = 0..03, 0.05, 0.10, 0.20, 0.30 s, K_{TC} = 0, excitations by fault-parallel displacement d_N (top two levels) and fault-normal pulse d_F (bottom two levels) and magnitudes M = 4 and 7, for the bridge models with pins over the columns (left) and in the central span (right)

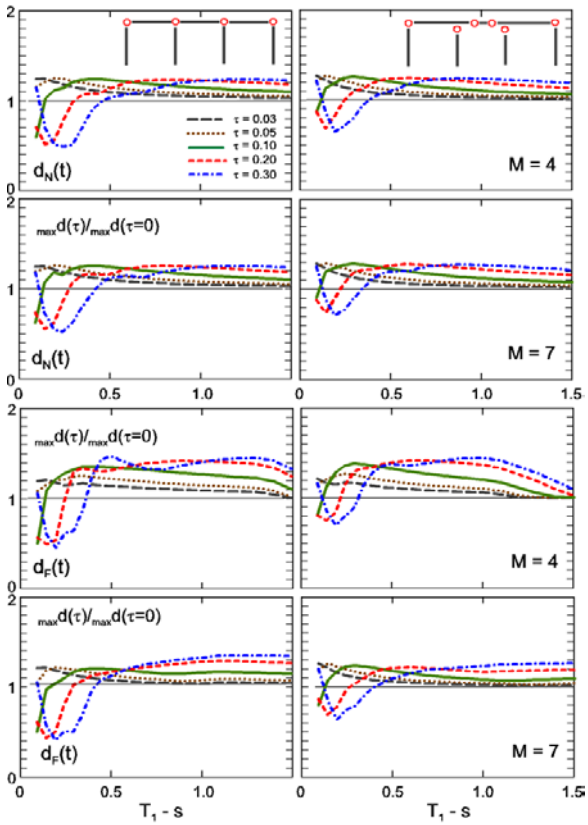

Fig. 4 Magnification factors of maximum linear drift in the piers of the bridge versus system fundamental period T_1 for time lag τ = 0..03, 0.05, 0.10, 0.20, 0.30 s, K_{TC} = 0, excitations by fault-parallel displacement d_N (top two levels) and fault-normal pulse d_F (bottom two levels) and magnitudes M = 4 and 7, for the bridge models with pins over the columns (left) and in the central span (right)

It is seen from Figure 2 that the same trends in the response are present as in Figure 1(a) of the paper by Jalali et al. (2012). It is seen that the maximum shear key forces and drifts in the piers induced by the fault-normal pulses are more than those induced by the fault-parallel displacements. With an increase in the main period of the bridge, the maximum shear key force decreases, while the maximum drift in the piers increases. For the excitation by a fault-parallel displacement, the maximum shear key forces and drifts in piers may increase up to 2g and 10 percent for stiff and soft bridges with T_1 = 0.1 and 1.5 s, respectively. Meanwhile, for the excitation by a fault-normal pulse, the corresponding values may increase up to 2g and 25 percent, respectively.

In Figures 3 and 4 we show the effects of wave passage on the maximum shear key forces and drifts in the piers of bridge for different earthquake magnitudes. As seen from Figure 3 under the near-fault ground motions, the differential motion effect on the maximum shear key forces of the bridge is negligible in the entire range of considered periods. Meanwhile, the wave passage of the translational out-of-plane excitation is seen to increase drifts by 25 to 40 percent for all magnitudes, and depending on the time delay and due to the combined action of out-of-plane and torsional responses, this amplification can occur in the entire range of considered periods (i.e., 0.1 < T_1 < 1.5).

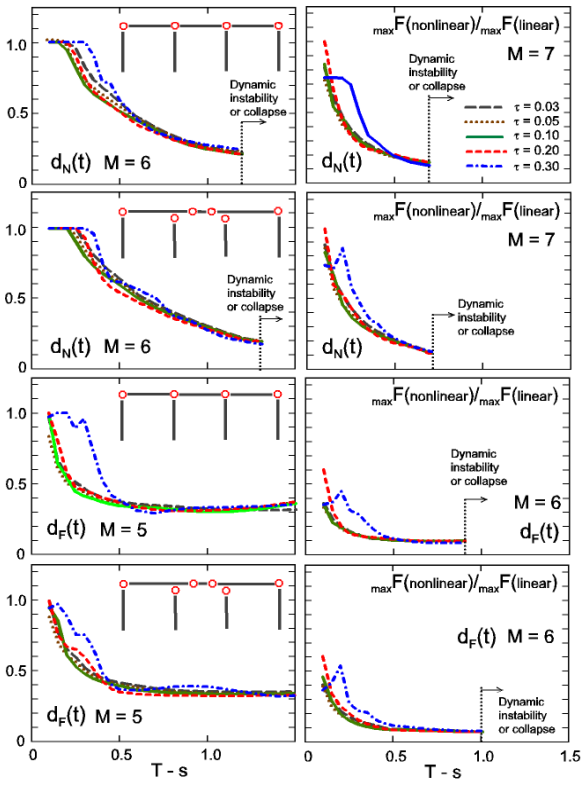

Fig. 5 Ratios of nonlinear maxima to linear maxima for the shear-key forces versus system fundamental period T_1 for time lag τ = 0..03, 0.05, 0.10, 0.20, 0.30 s, K_{TC} = 0, ϕ_y = 0.005, excitations by fault-parallel displacement d_N with magnitudes M = 6 and 7 (top two levels) and fault-normal pulse d_F with magnitudes M = 5 and 6 (bottom two levels), for the bridge models with pins over the columns (first and third levels from the top) and in the central span (second and fourth levels from the top)

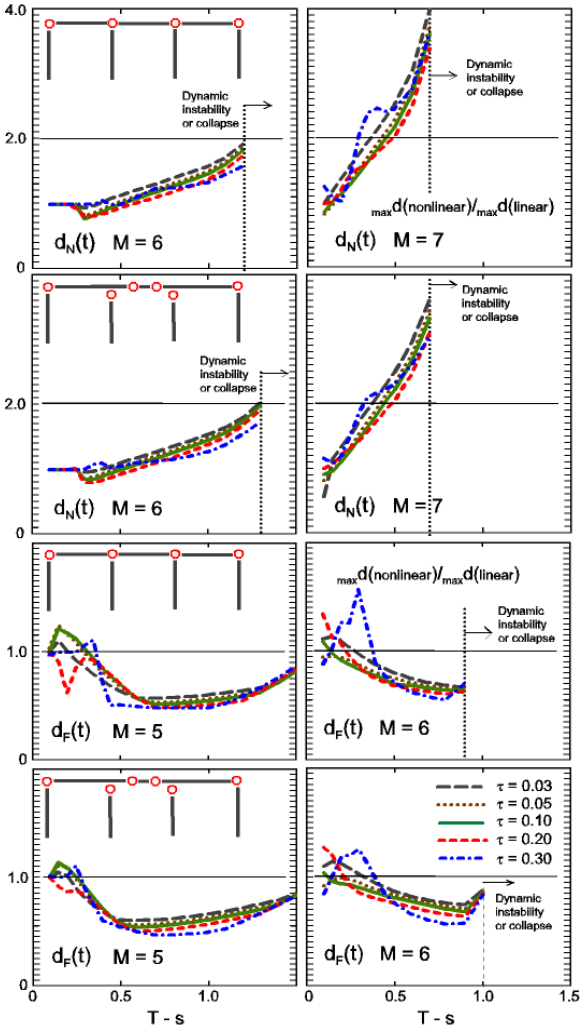

Fig. 6 Ratios of nonlinear maxima to linear maxima for drifts in the piers of the bridge versus system fundamental period T_1 for time lag τ = 0..03, 0.05, 0.10, 0.20, 0.30 s, K_{TC} = 0, ϕ_y = 0.005, excitations by fault-parallel displacement d_N with magnitudes M = 6 and 7 (top two levels) and fault-normal pulse d_F with magnitudes M = 5 and 6 (bottom two levels), for the bridge models with pins over the columns (first and third levels from the top) and in the central span (second and fourth levels from the top)

While assuming material nonlinearity in the bending of piers, we show the ratio of nonlinear to linear responses of the bridge in Figures 5–8. Again, we find the same trends as for the model in Figure 1(a). Depending on the main period of the bridge, earthquake magnitude and ϕ_y, the amplitude of the response become sensitive to the action of the gravity load. For large magnitudes and small ϕ_y values, the destabilizing effect of gravity and horizontal excitation leads to the conditions close to collapse (i.e., $\phi > \phi_s$). As seen from Figures 5–8, under the near-fault ground motions, the nonlinear behaviour of the piers

tends to decrease the maximum shear key forces relative to what occurs in the linear system. For the excitation by the fault-parallel displacements, the nonlinear behaviour of the piers leads to an increase in the maximum drift in the piers of the bridge. Meanwhile, under the fault-normal pulses, this trend is not observed and the nonlinear behaviour of the piers leads to a decrease in the maximum drift in the range of considered periods.

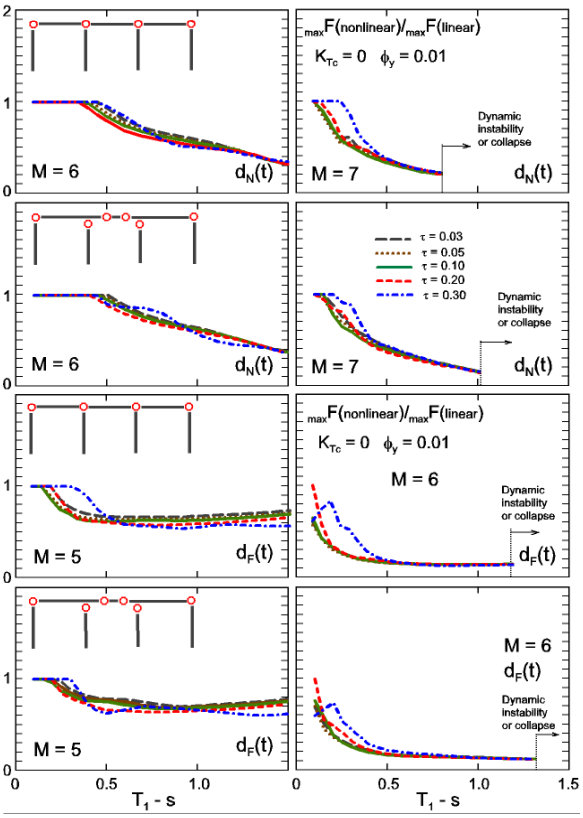

Fig. 7 Ratios of nonlinear maxima to linear maxima for the shear-key forces versus system fundamental period T_1 for time lag τ = 0..03, 0.05, 0.10, 0.20, 0.30 s, K_{TC} = 0, ϕ_y = 0.01, excitations by fault-parallel displacement d_N with magnitudes M = 6 and 7 (top two levels) and fault-normal pulse d_F with magnitudes M = 5 and 6 (bottom two levels), for the bridge models with pins over the columns (first and third levels from the top) and in the central span (second and fourth levels from the top)

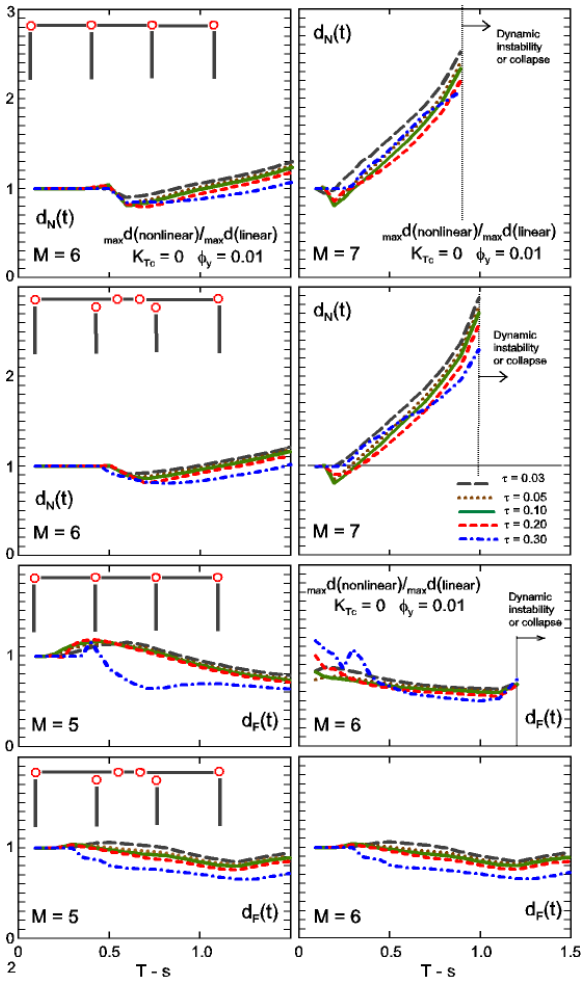

Fig. 8 Ratios of nonlinear maxima to linear maxima for drifts in the piers of the bridge versus system fundamental period T_1 for time lag τ = 0..03, 0.05, 0.10, 0.20, 0.30 s, K_{TC} = 0, ϕ_y = 0.01, excitations by fault-parallel displacement d_N with magnitudes M = 6 and 7 (top two levels) and fault-normal pulse d_F with magnitudes M = 5 and 6 (bottom two levels), for the bridge models with pins over the columns (first and third levels from the top) and in the central span (second and fourth levels from the top)

DISCUSSION AND CONCLUSIONS

The results of this study show that, with only a few exceptions, the key forces between the bridge piers and bridge decks are reduced for τ greater than zero relative to the synchronous excitation (corresponding to τ = 0), during the linear system response to the propagating excitations via the fault-parallel displacement d_N and fault-normal pulse d_F. The exceptions to this occur only in the end span (i.e., Span 4-2 in Figures 1(a) and 1(b)) and are associated with an out-of-plane whipping, as the displacements d_N and d_F leave the ground beneath the bridge and propagate out to the right. The reductions are more significant for the long transit times, i.e., τ longer than ~ 0.1 s, and mainly occur for the "stiff" piers corresponding to T_1 approximately between 0.1 and 0.3 s. This is due to the ability of the deck to deform by following an out-of-plane ground motion via relative rotation of the decks about the vertical axes through the piers at the pins 3 and 4 (see Figures 1(a) and 1(b)). As expected, these reductions become smaller and magnification factors become larger than 1 for very small T_1, when the torsional stiffness between the adjacent decks increases (Jalali et al., 2012). Also, the results of the simply supported model show that the wave-passage effects lead to the increases of about 25% to 40% in the drift of piers.

In the absence of pins, a long and continuous deck would have resulted in larger shear forces and bending moments in the piers during an out-of-plane excitation with non-zero transit times (Jalali and Trifunac, 2011; Jalali et al., 2012; Trifunac and Gicev, 2006). Such decks have large inertia and, through their large longitudinal rigidity, they force the entire relative displacement between the deck and the ground to be contributed by the piers. The rigid girders thus place larger demands on the piers.

The forces in the shear keys for the bridge models in Figures 1(a) and 1(b) are further reduced by significant amounts due to the nonlinear response of the piers (see Figures 5–8), as long as the drifts in the piers remain smaller than those values, which lead to the collapse caused by the gravity loads, dynamic instability, or both. Thus, it has been shown once again that for bridges and long structures on multiple supports, the internal forces can be significantly reduced by selecting those structural systems that can deform and conform to the motions imposed by the ground waves.

APPENDIX I: MODEL AND GOVERNING EQUATIONS OF BRIDGE

Shown in Figure A.1(a) is the model we consider in this paper. It is essentially the same model as the one studied by Jalali et al. (2012), with the only difference being the location of the pins in the central span. Previously, those pins were located above the columns, while in this paper they are at the distances a and b from the left and right supports of the central span. Consequently, the following formulation of the equilibrium equations is almost identical to the formulation presented in Appendix A of Jalali et al. (2012). Nevertheless, for completeness of this presentation, we include the corresponding equations for the model studied here and again outline the method of solution. We define the parameters of the model as follows:

$k_\phi =$ initial bending stiffness of the piers;

$c_\phi =$ linear bending damping coefficient of the piers;

$k_{T_c} =$ initial torsional stiffness of the piers;

$c_{T_c} =$ linear torsional damping coefficient of the piers;

$m_i =$ mass of the *i*th rigid deck;

$m = m_1 + m_2 + m_3 =$ total mass of the bridge;

$L_1 = L_2 = L_3 = L =$ length of each span of the bridge;

$a = b = L/5 =$ distance between the middle hinge and the nearest pier;

$J_i =$ polar moment of inertia of the *i*th rigid deck;

$h =$ height of the bridge;

ϕ_i = rotational angle of the *i*th pier;

v_{g_i}, θ_{g_i} = free-field out-of-plane and torsional motions of the ground surface at the base of the *i*th pier (i = 1, 2, 3, 4);

V_{G_i}, θ_{G_i} = absolute out-of-plane and torsional motions of the center of gravity of the *i*th rigid deck (i = 1, 2, 3); and

F_a, F_b = forces in the shear keys at the middle hinges.

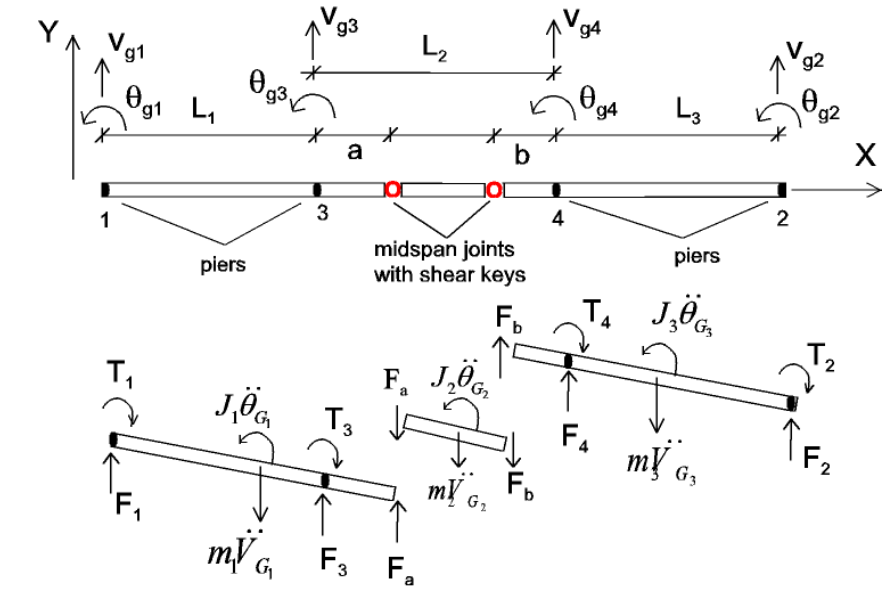

(a)

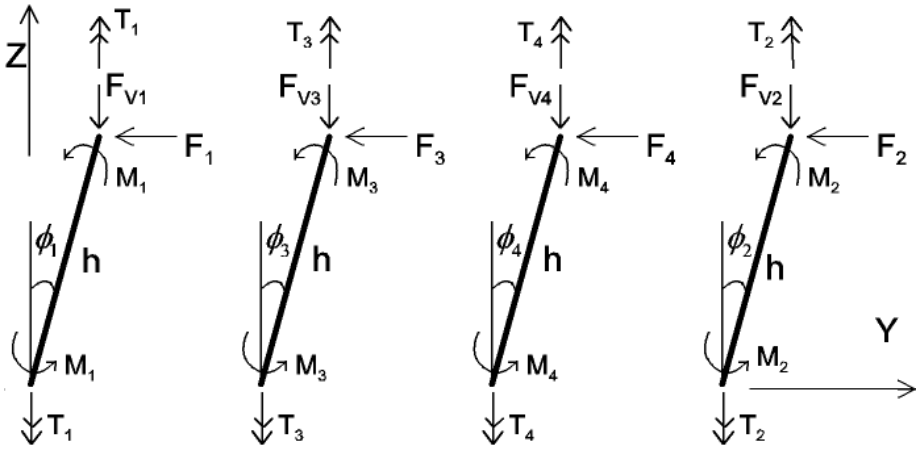

(b)

Fig. A.1 (a) Plan view of the bridge; (b) Side view of the bridge piers and of the forces acting on them

From the geometry of the model (see Figures A.1(a) and A.1(b)), the absolute out-of-plane displacement and torsional rotation of the center of gravity of the three rigid decks are obtained as

$$V_{G_1} = \frac{L-a}{2L}V_1 + \frac{L+a}{2L}V_3 = \frac{L-a}{2L}\left(V_{g_1} + h\sin\phi_1\right) + \frac{L+a}{2L}\left(V_{g_3} + h\sin\phi_3\right) \tag{A.1a}$$

$$V_{G_3} = \frac{L-a}{2L}V_2 + \frac{L+b}{2L}V_4 = \frac{L-b}{2L}\left(V_{g_2} + h\sin\phi_2\right) + \frac{L+b}{2L}\left(V_{g_4} + h\sin\phi_4\right) \tag{A.1b}$$

$$V_a = \frac{-a}{L}\left(V_{g_1} + h\sin\phi_1\right) + \frac{L+a}{L}\left(V_{g_3} + h\sin\phi_3\right) \tag{A.1c}$$

$$V_b = \frac{-b}{L}\left(V_{g_2} + h\sin\phi_2\right) + \frac{L+b}{L}\left(V_{g_4} + h\sin\phi_4\right) \tag{A.1d}$$

$$V_{G_2} = \frac{V_a + V_b}{2} = \frac{-a}{2L}\left(V_{g_1} + h\sin\phi_1\right) - \frac{b}{2L}\left(V_{g_2} + h\sin\phi_2\right) + \frac{L+a}{2L}\left(V_{g_3} + h\sin\phi_3\right) + \frac{L+b}{2L}\left(V_{g_4} + h\sin\phi_4\right) \tag{A.1e}$$

$$\theta_{G_1} = \sin^{-1}\left(\frac{V_1 - V_3}{L}\right) = \sin^{-1}\left\{\frac{1}{L}\left[\left(V_{g_1} - V_{g_3}\right) + h\left(\sin\phi_1 - \sin\phi_3\right)\right]\right\} \tag{A.1f}$$

$$\theta_{G_2} = \sin^{-1}\left\{\frac{-a\left(V_{g_1} + h\sin\phi_1\right) + b\left(V_{g_2} + h\sin\phi_2\right) + \left(L+a\right)\left(V_{g_3} + h\sin\phi_3\right) - \left(L+b\right)\left(V_{g_4} + h\sin\phi_4\right)}{L\left[L - \left(a+b\right)\right]}\right\} \tag{A.1g}$$

$$\theta_{G_3} = \sin^{-1}\left(\frac{V_4 - V_2}{L}\right) = \sin^{-1}\left\{\frac{1}{L}\left[\left(V_{g_4} - V_{g_2}\right) + h\left(\sin\phi_4 - \sin\phi_2\right)\right]\right\} \tag{A.1h}$$

On differentiating these with respect to time, we obtain

$$\dot{V}_{G_1} = \frac{L-a}{2L}\left(\dot{V}_{g_1} + h\cos\phi_1\dot{\phi}_1\right) + \frac{L+a}{2L}\left(\dot{V}_{g_3} + h\cos\phi_3\dot{\phi}_3\right) \tag{A.2a}$$

$$\ddot{V}_{G_1} = \frac{L-a}{2L}\left(\ddot{V}_{g_1} - h\sin\phi_1\dot{\phi}_1^2 + h\cos\phi_1\ddot{\phi}_1\right) + \frac{L+a}{2L}\left(\ddot{V}_{g_3} - h\sin\phi_3\dot{\phi}_3^2 + h\cos\phi_3\ddot{\phi}_3\right) \tag{A.2b}$$

$$\dot{\theta}_{G_1} = \frac{\left[\left(\dot{V}_{g_1} - \dot{V}_{g_3}\right) + h\left(\cos\phi_1\dot{\phi}_1 - \cos\phi_3\dot{\phi}_3\right)\right]}{L\cos\theta_{G_1}} \tag{A.2c}$$

$$\ddot{\theta}_{G_1} = \frac{\left[\left(\ddot{V}_{g_1} - \ddot{V}_{g_3}\right) + h\left(\cos\phi_1\ddot{\phi}_1 - \sin\phi_1\dot{\phi}_1^2 - \cos\phi_3\ddot{\phi}_3 + \sin\phi_3\dot{\phi}_3^2\right)\right]}{L\cos\theta_{G_1}} + \tan\theta_{G_1}\dot{\theta}_{G_1}^2 \tag{A.2d}$$

$$\dot{V}_{G_2} = \frac{-a}{2L}\left(\dot{V}_{g_1} + h\cos\phi_1\dot{\phi}_1\right) - \frac{b}{2L}\left(\dot{V}_{g_2} + h\cos\phi_2\dot{\phi}_2\right) + \frac{L+a}{2L}\left(\dot{V}_{g_3} + h\cos\phi_3\dot{\phi}_3\right) + \frac{L+b}{2L}\left(\dot{V}_{g_4} + h\cos\phi_4\dot{\phi}_4\right) \tag{A.2e}$$

$$\ddot{V}_{G_2} = \frac{-a}{2L}\left(\ddot{V}_{g_1} - h\sin\phi_1\dot{\phi}_1^2 + h\cos\phi_1\ddot{\phi}_1\right) - \frac{b}{2L}\left(\ddot{V}_{g_2} - h\sin\phi_2\dot{\phi}_2^2 + h\cos\phi_2\ddot{\phi}_2\right) + \frac{L+a}{2L}\left(\ddot{V}_{g_3} - h\sin\phi_3\dot{\phi}_3^2 + h\cos\phi_3\ddot{\phi}_3\right) + \frac{L+b}{2L}\left(\ddot{V}_{g_4} - h\sin\phi_4\dot{\phi}_4^2 + h\cos\phi_4\ddot{\phi}_4\right) \tag{A.2f}$$

$$\dot{\theta}_{G_2} = \frac{1}{L\left[L - \left(a+b\right)\right]\cos\theta_{G_2}}\left[-a\left(\dot{V}_{g_1} + h\cos\phi_1\dot{\phi}_1\right) + b\left(\dot{V}_{g_2} + h\cos\phi_2\dot{\phi}_2\right) + \left(L+a\right)\left(\dot{V}_{g_3} + h\cos\phi_3\dot{\phi}_3\right) - \left(L+b\right)\left(\dot{V}_{g_4} + h\cos\phi_4\dot{\phi}_4\right)\right] \tag{A.2g}$$

$$\ddot{\theta}_{G_2} = \frac{1}{L\left[L-(a+b)\right]\cos\theta_{G_2}}\Big[-a\left(\ddot{V}_{g_1} + h\cos\phi_1\ddot{\phi}_1 - h\sin\phi_1\dot{\phi}_1^2\right) + b\left(\ddot{V}_{g_2} + h\cos\phi_2\ddot{\phi}_2 - h\sin\phi_2\dot{\phi}_2^2\right) + (L+a)\left(\ddot{V}_{g_3} + h\cos\phi_3\ddot{\phi}_3 - h\sin\phi_3\dot{\phi}_3^2\right) - (L+b)\left(\ddot{V}_{g_4} + h\cos\phi_4\ddot{\phi}_4 - h\sin\phi_4\dot{\phi}_4^2\right)\Big] + \tan\theta_{G_2}\dot{\theta}_{G_2}^2 \quad \text{(A.2h)}$$

$$\dot{V}_{G_3} = \frac{L-b}{2L}\left(\dot{V}_{g_2} + h\cos\phi_2\dot{\phi}_2\right) + \frac{L+b}{2L}\left(\dot{V}_{g_4} + h\cos\phi_4\dot{\phi}_4\right) \quad \text{(A.2i)}$$

$$\ddot{V}_{G_3} = \frac{L-b}{2L}\left(\ddot{V}_{g_2} - h\sin\phi_2\dot{\phi}_2^2 + h\cos\phi_2\ddot{\phi}_2\right) + \frac{L+b}{2L}\left(\ddot{V}_{g_4} - h\sin\phi_4\dot{\phi}_4^2 + h\cos\phi_4\ddot{\phi}_4\right) \quad \text{(A.2j)}$$

$$\dot{\theta}_{G_3} = \frac{\left(\dot{V}_{g_4} - \dot{V}_{g_2}\right) + h\left(\cos\phi_4\dot{\phi}_4 - \cos\phi_2\dot{\phi}_2\right)}{L\cos\theta_{G_3}} \quad \text{(A.2k)}$$

$$\ddot{\theta}_{G_3} = \frac{\left(\ddot{V}_{g_4} - \ddot{V}_{g_2}\right) + h\left(\cos\phi_4\ddot{\phi}_4 - \sin\phi_4\dot{\phi}_4^2 - \cos\phi_2\ddot{\phi}_2 + \sin\phi_2\dot{\phi}_2^2\right)}{L\cos\theta_{G_3}} + \tan\theta_{G_3}\dot{\theta}_{G_3}^2 \quad \text{(A.2l)}$$

The equilibrium equations of the three rigid decks are obtained from $\sum F = 0$ and $\sum M_G = 0$ as

$$F_1 + F_3 + F_a - m_1\ddot{V}_{G_1} = 0 \quad \text{(A.3a)}$$

$$F_a + F_b + m_2\ddot{V}_{G_2} = 0 \quad \text{(A.3b)}$$

$$F_b + F_4 + F_2 - m_3\ddot{V}_{G_3} = 0 \quad \text{(A.3c)}$$

$$T_1 + T_3 + F_1\frac{L+a}{2}\cos\theta_{G_1} - J_1\ddot{\theta}_{G_1} - F_3\frac{L-a}{2}\cos\theta_{G_1} - F_a\frac{L+a}{2}\cos\theta_{G_1} = 0 \quad \text{(A.3d)}$$

$$\left(F_b - F_a\right)\frac{L-(a+b)}{2}\cos\theta_{G_2} - J_2\ddot{\theta}_{G_2} = 0 \quad \text{(A.3e)}$$

$$T_2 + T_4 + F_b\frac{L+b}{2}\cos\theta_{G_3} + F_4\frac{L-b}{2}\cos\theta_{G_3} - F_2\frac{L+b}{2}\cos\theta_{G_3} - J_3\ddot{\theta}_{G_3} = 0 \quad \text{(A.3f)}$$

On substituting Equations (A.3a) and (A.3c) into other equations we find the independent equations of motion of the system as

$$-F_1 - F_2 - F_3 - F_4 + m_1\ddot{V}_{G_1} + m_2\ddot{V}_{G_2} + m_3\ddot{V}_{G_3} = 0 \quad \text{(A.4a)}$$

$$T_1 + T_3 + F_1\left(L+a\right)\cos\theta_{G_1} + F_3 a\cos\theta_{G_1} - m_1\ddot{V}_{G_1}\frac{L+a}{2}\cos\theta_{G_1} - J_1\ddot{\theta}_{G_1} = 0 \quad \text{(A.4b)}$$

$$\left(m_3\ddot{V}_{G_3} + F_1 + F_3 - m_1\ddot{V}_{G_1} - F_2 - F_4\right)\frac{L-a-b}{2}\cos\theta_{G_2} = 0 \quad \text{(A.4c)}$$

$$T_2 + T_4 - F_2\left(L+b\right)\cos\theta_{G_3} - F_4 b\cos\theta_{G_3} - m_3\ddot{V}_{G_3}\frac{L+b}{2}\cos\theta_{G_3} - J_3\ddot{\theta}_{G_3} = 0 \quad \text{(A.4d)}$$

The equilibrium equation of the *i*th pier follows from $\sum M = 0$ as

$$2M_i + F_i h\cos\phi_i - F_{V_i} h\sin\phi_i = 0 \quad \Rightarrow \quad F_i = F_{V_i}\tan\phi_i - \frac{2M_i}{h\cos\phi_i} \quad \text{(A.5)}$$

Assuming a uniform distribution of mass over the length of the bridge decks, we approximately determine F_{V_i} as

$$F_{V_1} = \left[\frac{m_1}{2} - \left(m_1 + m_2\right)\frac{a}{2L}\right]g \tag{A.6a}$$

$$F_{V_2} = \left[\frac{m_3}{2} - \left(m_2 + m_3\right)\frac{b}{2L}\right]g \tag{A.6b}$$

$$F_{V_3} = \left(m_1 + m_2\right)\frac{L+a}{2L}g \tag{A.6c}$$

$$F_{V_4} = \left(m_2 + m_3\right)\frac{L+b}{2L}g \tag{A.6d}$$

The bending and torsional moments of piers are then defined as (see Figures A.2(a) and A.2(b))

$$M_i = K_\phi F(\phi_i) + C_\phi \dot{\phi}_i \tag{A.7a}$$

$$T_1 = K_{T_C}\Phi\left(\theta_{g_1} - \theta_{G_1}\right) + C_{T_C}\left(\dot{\theta}_{g_1} - \dot{\theta}_{G_1}\right) \tag{A.7b}$$

$$T_2 = K_{T_C}\Phi\left(\theta_{g_2} - \theta_{G_3}\right) + C_{T_C}\left(\dot{\theta}_{g_2} - \dot{\theta}_{G_3}\right) \tag{A.7c}$$

$$T_3 = K_{T_C}\Phi\left(\theta_{g_3} - \theta_{G_1}\right) + C_{T_C}\left(\dot{\theta}_{g_3} - \dot{\theta}_{G_1}\right) \tag{A.7d}$$

$$T_4 = K_{T_C}\Phi\left(\theta_{g_4} - \theta_{G_3}\right) + C_{T_C}\left(\dot{\theta}_{g_4} - \dot{\theta}_{G_3}\right) \tag{A.7e}$$

Here, $F(\phi)$ and $\Phi(\phi)$ are the nonlinear functions of the type described in Figure A.3.

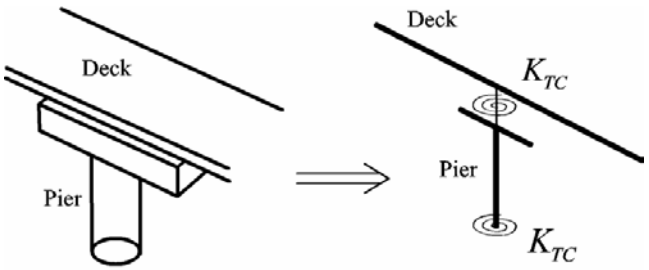

(a)

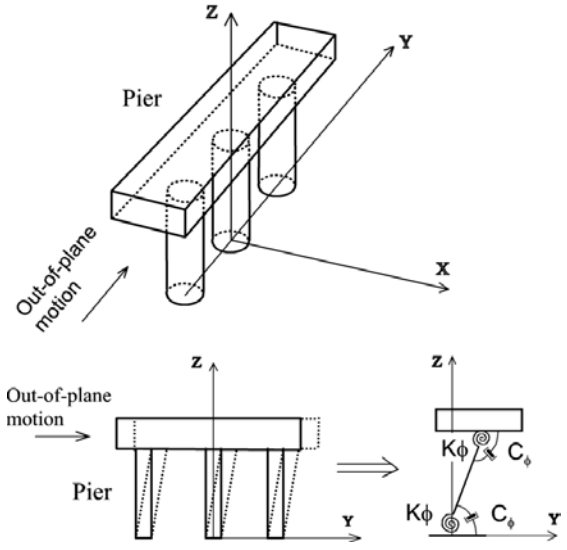

(b)

Fig. A.2 (a) Schematic representations of torsional stiffness between the pier and the ground and between the pier and the deck; (b) Schematic representation of the deformation of a pier and of the associated stiffness and damping

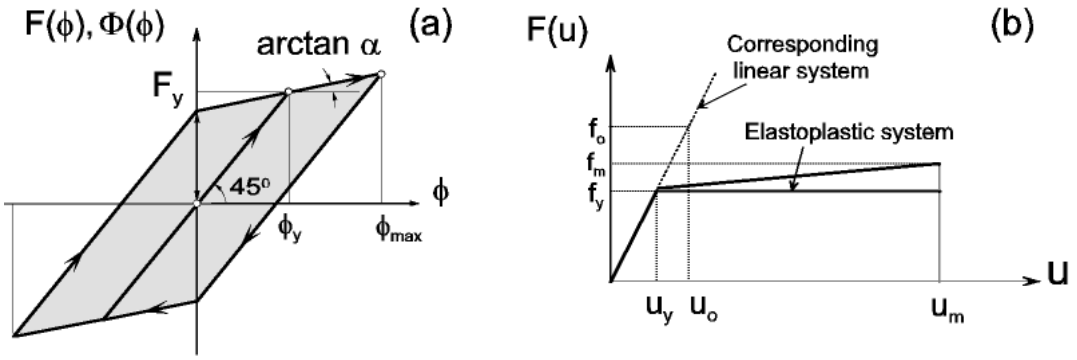

Fig. A.3 Force-displacement and moment-rotation relationship for the bilinear spring

Using Equations (A.2a)–(A.2l), (A.5), (A.6a)–(A.6d) and (A.7a)–(A.7e), one can write independent equations with respect to ϕ_1, ϕ_2, ϕ_3 and ϕ_4 as

$$\begin{aligned}
&\left[-m_1(L-a)+m_2a\right]\frac{h\cos\phi_1}{2L}\ddot{\phi}_1+\left[m_2b-m_3(L-b)\right]\frac{h\cos\phi_2}{2L}\ddot{\phi}_2-(m_1+m_2)\frac{L+a}{2L}h\cos\phi_3\ddot{\phi}_3\\
&-(m_2+m_3)\frac{L+b}{2L}h\cos\phi_4\ddot{\phi}_4+\left[\frac{m_1}{2}-(m_1+m_2)\frac{a}{2L}\right]g\tan\phi_1-\frac{2M_1}{h\cos\phi_1}\\
&+\left[\frac{m_3}{2}-(m_2+m_3)\frac{b}{2L}\right]g\tan\phi_2-\frac{2M_2}{h\cos\phi_2}+(m_1+m_2)\frac{L+a}{2L}g\tan\phi_3-\frac{2M_3}{h\cos\phi_3}\\
&+(m_2+m_3)\frac{L+b}{2L}g\tan\phi_4-\frac{2M_4}{h\cos\phi_4}-\frac{m_1(L-a)}{2L}\left(\ddot{V}_{g_1}-h\sin\phi_1\dot{\phi}_1^2\right)\\
&-\frac{m_1(L+a)}{2L}\left(\ddot{V}_{g_3}-h\sin\phi_3\dot{\phi}_3^2\right)+\frac{m_2a}{2L}\left(\ddot{V}_{g_1}-h\sin\phi_1\dot{\phi}_1^2\right)+\frac{m_2b}{2L}\left(\ddot{V}_{g_2}-h\sin\phi_2\dot{\phi}_2^2\right)\\
&-\frac{m_2(L+a)}{2L}\left(\ddot{V}_{g_3}-h\sin\phi_3\dot{\phi}_3^2\right)-\frac{m_2(L+b)}{2L}\left(\ddot{V}_{g_4}-h\sin\phi_4\dot{\phi}_4^2\right)\\
&-\frac{m_3(L-b)}{2L}\left(\ddot{V}_{g_2}-h\sin\phi_2\dot{\phi}_2^2\right)-\frac{m_3(L+b)}{2L}\left(\ddot{V}_{g_4}-h\sin\phi_4\dot{\phi}_4^2\right)=0
\end{aligned}\tag{A.8a}$$

$$\begin{aligned}
&\left[\frac{-m_1(L^2-a^2)}{4L}\cos\theta_{G_1}-\frac{J_1}{L\cos\theta_{G_1}}\right]h\cos\phi_1\ddot{\phi}_1+\left[\frac{-m_1(L+a)^2}{4L}\cos\theta_{G_1}+\frac{J_1}{L\cos\theta_{G_1}}\right]h\cos\phi_3\ddot{\phi}_3+\\
&+K_{T_C}\Phi\left(\theta_{g_1}-\theta_{G_1}\right)+C_{T_C}\left(\dot{\theta}_{g_1}-\dot{\theta}_{G_1}\right)+K_{T_C}\Phi\left(\theta_{g_3}-\theta_{G_1}\right)+C_{T_C}\left(\dot{\theta}_{g_3}-\dot{\theta}_{G_1}\right)\\
&-\frac{2M_1}{h\cos\phi_1}(L+a)\cos\theta_{G_1}+\left[\frac{m_1}{2}-(m_1+m_2)\frac{a}{2L}\right]g(L+a)\cos\theta_{G_1}\tan\phi_1\\
&+\left[(m_1+m_2)\frac{L+a}{2L}ga\cos\theta_{G_1}\tan\phi_3\right]-\frac{2M_3}{h\cos\phi_3}a\cos\theta_{G_1}\\
&-\frac{m_1(L^2-a^2)}{4L}\cos\theta_{G_1}\left(\ddot{V}_{g_1}-h\sin\phi_1\dot{\phi}_1^2\right)-\frac{m_1(L+a)^2}{4L}\cos\theta_{G_1}\left(\ddot{V}_{g_3}-h\sin\phi_3\dot{\phi}_3^2\right)\\
&-\frac{J_1}{L\cos\theta_{G_1}}\left(\ddot{V}_{g_1}-\ddot{V}_{g_3}-h\sin\phi_1\dot{\phi}_1^2+h\sin\phi_3\dot{\phi}_3^2\right)-J_1\tan\theta_{G_1}\dot{\theta}_{G_1}^2=0
\end{aligned}\tag{A.8b}$$

$$\left[\frac{-m_1(L-a)}{2L}\frac{L-(a+b)}{2}\cos\theta_{G_2}+\frac{J_2 a}{L(L-a-b)\cos\theta_{G_2}}\right]h\cos\phi_1\ddot{\phi}_1$$
$$+\left[\frac{m_3(L-b)}{2L}\frac{L-(a+b)}{2}\cos\theta_{G_2}-\frac{J_2 b}{L(L-a-b)\cos\theta_{G_2}}\right]h\cos\phi_2\ddot{\phi}_2$$
$$+\left[\frac{-m_1(L+a)}{2L}\frac{L-a-b}{2}\cos\theta_{G_2}-\frac{J_2(L+a)}{L(L-a-b)\cos\theta_{G_2}}\right]h\cos\phi_3\ddot{\phi}_3$$
$$+\left[\frac{m_3(L+b)}{2L}\frac{L-a-b}{2}\cos\theta_{G_2}+\frac{J_2(L+a)}{L(L-a-b)\cos\theta_{G_2}}\right]h\cos\phi_4\ddot{\phi}_4$$
$$+\frac{m_3(L-b)(L-a-b)}{4L}\cos\theta_{G_2}\left(\ddot{V}_{g_2}-h\sin\phi_2\dot{\phi}_2^2\right)$$
$$+\frac{m_3(L+b)(L-a-b)}{4L}\cos\theta_{G_2}\left(\ddot{V}_{g_4}-h\sin\phi_4\dot{\phi}_4^2\right)$$
$$+\left\{\left[\frac{m_1}{2}-(m_1+m_2)\frac{a}{2L}\right]g\tan\phi_1-\frac{2M_1}{h\cos\phi_1}-\left[\frac{m_3}{2}-(m_2+m_3)\frac{b}{2L}\right]g\tan\phi_2\right. \tag{A.8c}$$
$$+\frac{2M_2}{h\cos\phi_2}+\frac{(m_1+m_2)(L+a)}{2L}g\tan\phi_3-\frac{2M_3}{h\cos\phi_3}+\frac{2M_4}{h\cos\phi_4}$$
$$-\frac{(m_2+m_3)(L+b)}{2L}g\tan\phi_4-\frac{m_1(L-a)}{2L}\left(\ddot{V}_{g_1}-h\sin\phi_1\dot{\phi}_1^2\right)$$
$$\left.-\frac{m_1(L+a)}{2L}\left(\ddot{V}_{g_3}-h\sin\phi_3\dot{\phi}_3^2\right)\right\}\frac{L-a-b}{2}\cos\theta_{G_2}$$
$$-\frac{J_2}{L(L-a-b)\cos\theta_{G_2}}\left[-a\left(\ddot{V}_{g_1}-h\sin\phi_1\dot{\phi}_1^2\right)\right.$$
$$+b\left(\ddot{V}_{g_2}-h\sin\phi_2\dot{\phi}_2^2\right)+(L+a)\left(\ddot{V}_{g_3}-h\sin\phi_3\dot{\phi}_3^2\right)$$
$$\left.-(L+b)\left(\ddot{V}_{g_4}-h\sin\phi_4\dot{\phi}_4^2\right)\right]-J_2\tan\theta_{G_2}\dot{\theta}_{G_2}^2=0$$

$$\left[\frac{m_3(L^2-b^2)}{4L}\cos\theta_{G_3}+\frac{J_3}{L\cos\theta_{G_3}}\right]h\cos\phi_2\ddot{\phi}_2+\left[\frac{m_3(L+b)^2}{4L}\cos\theta_{G_3}-\frac{J_3}{L\cos\theta_{G_3}}\right]h\cos\phi_4\ddot{\phi}_4$$
$$+K_{T_C}\Phi\left(\theta_{g_2}-\theta_{G_3}\right)+C_{T_C}\left(\dot{\theta}_{g_2}-\dot{\theta}_{G_3}\right)+K_{T_C}\Phi\left(\theta_{g_4}-\theta_{G_3}\right)+C_{T_C}\left(\dot{\theta}_{g_4}-\dot{\theta}_{G_3}\right)$$
$$-\left[\left(\frac{m_3}{2}-(m_2+m_3)\frac{b}{2L}\right)g\tan\phi_2-\frac{2M_2}{h\cos\phi_2}\right](L+b)\cos\theta_{G_3}-\left[(m_2+m_3)\frac{L+b}{2L}g\tan\phi_4\right. \tag{A.8d}$$
$$\left.-\frac{2M_4}{h\cos\phi_4}\right]b\cos\theta_{G_3}+\frac{m_3(L^2-b^2)}{4L}\cos\theta_{G_3}\left(\ddot{V}_{g_2}-h\sin\phi_2\dot{\phi}_2\right)$$
$$+\frac{m_3(L+b)^2}{4L}\cos\theta_{G_3}\left(\ddot{V}_{g_4}-h\sin\phi_4\dot{\phi}_4^2\right)-\frac{J_3}{L\cos\theta_{G_3}}\left[\ddot{V}_{g_4}-\ddot{V}_{g_2}+h\left(-\sin\phi_4\dot{\phi}_4^2+\sin\phi_2\dot{\phi}_2^2\right)\right]$$
$$-J_3\tan\theta_{G_3}\dot{\theta}_{G_3}^2=0$$

By considering

$$m = m_1 + m_2 + m_3 \tag{A.9a}$$

$$\alpha_{m_i} = \frac{m_i}{m} \tag{A.9b}$$

the above equations can be written in the matrix form as

$$\begin{bmatrix} c_{11} & c_{12} & c_{13} & c_{14} \\ c_{21} & c_{22} & c_{23} & c_{24} \\ c_{31} & c_{32} & c_{33} & c_{34} \\ c_{41} & c_{42} & c_{43} & c_{44} \end{bmatrix} \begin{Bmatrix} \ddot{\phi}_1 \\ \ddot{\phi}_2 \\ \ddot{\phi}_3 \\ \ddot{\phi}_4 \end{Bmatrix} + \begin{Bmatrix} c_{15} \\ c_{25} \\ c_{35} \\ c_{45} \end{Bmatrix} = \begin{Bmatrix} 0 \\ 0 \\ 0 \\ 0 \end{Bmatrix} \tag{A.10}$$

where,

$$c_{11} = \left[\alpha_{m_1}(L-a) - \alpha_{m_2} a\right] \frac{h\cos\phi_1}{2L} \tag{A.11a}$$

$$c_{12} = \left[-\alpha_{m_2} b + \alpha_{m_3}(L-b)\right] \frac{h\cos\phi_2}{2L} \tag{A.11b}$$

$$c_{13} = \left(\alpha_{m_1} + \alpha_{m_2}\right) \frac{L+a}{2L} h\cos\phi_3 \tag{A.11c}$$

$$c_{14} = \left(\alpha_{m_2} + \alpha_{m_3}\right) \frac{L+b}{2L} h\cos\phi_4 \tag{A.11d}$$

$$\begin{aligned} c_{15} = {} & \left[\frac{-\alpha_{m_1}}{2} + \left(\alpha_{m_1} + \alpha_{m_2}\right)\frac{a}{2L}\right] g\tan\phi_1 + \frac{2M_1}{mh\cos\phi_1} + \left[\frac{-\alpha_{m_3}}{2} + \left(\alpha_{m_2} + \alpha_{m_3}\right)\frac{b}{2L}\right] g\tan\phi_2 \\ & + \frac{2M_2}{mh\cos\phi_2} - \left(\alpha_{m_1} + \alpha_{m_2}\right)\frac{L+a}{2L} g\tan\phi_3 + \frac{2M_3}{mh\cos\phi_3} - \left(\alpha_{m_2} + \alpha_{m_3}\right)\frac{L+b}{2L} g\tan\phi_4 \\ & + \frac{2M_4}{mh\cos\phi_4} + \frac{\alpha_{m_1}(L-a)}{2L}\left(\ddot{V}_{g_1} - h\sin\phi_1\dot{\phi}_1^2\right) + \frac{\alpha_{m_1}(L+a)}{2L}\left(\ddot{V}_{g_3} - h\sin\phi_3\dot{\phi}_3^2\right) \\ & - \frac{\alpha_{m_2} a}{2L}\left(\ddot{V}_{g_1} - h\sin\phi_1\dot{\phi}_1^2\right) - \frac{\alpha_{m_2} b}{2L}\left(\ddot{V}_{g_2} - h\sin\phi_2\dot{\phi}_2^2\right) + \frac{\alpha_{m_2}(L+a)}{2L}\left(\ddot{V}_{g_3} - h\sin\phi_3\dot{\phi}_3^2\right) \\ & + \frac{\alpha_{m_2}(L+b)}{2L}\left(\ddot{V}_{g_4} - h\sin\phi_4\dot{\phi}_4^2\right) + \frac{\alpha_{m_3}(L-b)}{2L}\left(\ddot{V}_{g_2} - h\sin\phi_2\dot{\phi}_2^2\right) \\ & + \frac{\alpha_{m_3}(L+b)}{2L}\left(\ddot{V}_{g_4} - h\sin\phi_4\dot{\phi}_4^2\right) \end{aligned} \tag{A.11e}$$

$$c_{21} = \left[\frac{-3(L-a)}{L(L+a)}\cos\theta_{G_1} - \frac{1}{L\cos\theta_{G_1}}\right] h\cos\phi_1 \tag{A.11f}$$

$$c_{22} = 0 \tag{A.11g}$$

$$c_{24} = 0 \tag{A.11h}$$

$$c_{23} = \left(\frac{-3}{L}\cos\theta_{G_1} + \frac{1}{L\cos\theta_{G_1}}\right) h\cos\phi_3 \tag{A.11i}$$

$$c_{25}=\frac{K_{T_C}}{J_1}\Phi\left(\theta_{g_1}-\theta_{G_1}\right)+\frac{C_{T_C}}{J_1}\left(\dot\theta_{g_1}-\dot\theta_{G_1}\right)+\frac{K_{T_C}}{J_1}\Phi\left(\theta_{g_3}-\theta_{G_1}\right)+\frac{C_{T_C}}{J_1}\left(\dot\theta_{g_3}-\dot\theta_{G_1}\right)$$
$$+6\left[1-\left(1+\frac{\alpha_{m_2}}{\alpha_{m_1}}\right)\frac{a}{L}\right]\frac{g\cos\theta_{G_1}}{L+a}\tan\phi_1-\frac{2M_1}{J_1h\cos\phi_1}\left(L+a\right)\cos\theta_{G_1}$$
$$+6\left(1+\frac{\alpha_{m_2}}{\alpha_{m_1}}\right)\frac{a}{L\left(L+a\right)}g\cos\theta_{G_1}\tan\phi_3-\frac{2M_3}{J_1h\cos\phi_3}a\cos\theta_{G_1} \tag{A.11j}$$
$$-\frac{3\left(L-a\right)}{L\left(L+a\right)}\cos\theta_{G_1}\left(\ddot V_{g_1}-h\sin\phi_1\dot\phi_1^2\right)-\frac{3}{L}\cos\theta_{G_1}\left(\ddot V_{g_3}-h\sin\phi_3\dot\phi_3^2\right)$$
$$-\frac{1}{L\cos\theta_{G_1}}\left(\ddot V_{g_1}-\ddot V_{g_3}-h\sin\phi_1\dot\phi_1^2+h\sin\phi_3\dot\phi_3^2\right)-\tan\theta_{G_1}\dot\theta_{G_1}^2$$

$$c_{31}=\left[\frac{-3\alpha_{m_1}}{\alpha_{m_2}}\frac{L-a}{L\left(L-a-b\right)}\cos\theta_{G_2}+\frac{a}{L\left(L-a-b\right)\cos\theta_{G_2}}\right]h\cos\phi_1 \tag{A.11k}$$

$$c_{32}=\left[\frac{3\alpha_{m_3}}{\alpha_{m_2}}\frac{L-b}{L\left(L-a-b\right)}\cos\theta_{G_2}-\frac{b}{L\left(L-a-b\right)\cos\theta_{G_2}}\right]h\cos\phi_2 \tag{A.11l}$$

$$c_{33}=\left[\frac{-3\alpha_{m_1}}{\alpha_{m_2}}\frac{L+a}{L\left(L-a-b\right)}\cos\theta_{G_2}-\frac{L+a}{L\left(L-a-b\right)\cos\theta_{G_2}}\right]h\cos\phi_3 \tag{A.11m}$$

$$c_{34}=\left[\frac{3\alpha_{m_3}}{\alpha_{m_2}}\frac{L+b}{L\left(L-a-b\right)}\cos\theta_{G_2}+\frac{L+b}{L\left(L-a-b\right)\cos\theta_{G_2}}\right]h\cos\phi_4 \tag{A.11n}$$

$$c_{35}=\frac{3\alpha_{m_3}}{\alpha_{m_2}}\frac{L-b}{L\left(L-a-b\right)}\cos\theta_{G_2}\left(\ddot V_{g_2}-h\sin\phi_2\dot\phi_2^2\right)+\frac{3\alpha_{m_3}}{\alpha_{m_2}}\frac{L+b}{L\left(L-a-b\right)}\cos\theta_{G_2}$$
$$\times\left(\ddot V_{g_4}-h\sin\phi_4\dot\phi_4^2\right)+\frac{3g}{L-a-b}\cos\theta_{G_2}\left\{\left[\frac{\alpha_{m_1}}{\alpha_{m_2}}-\left(\frac{\alpha_{m_1}}{\alpha_{m_2}}+1\right)\frac{a}{L}\right]\tan\phi_1\right.$$
$$\left.-\left[\frac{\alpha_{m_3}}{\alpha_{m_2}}-\left(1+\frac{\alpha_{m_3}}{\alpha_{m_2}}\right)\frac{b}{L}\right]\tan\phi_2+\left(\frac{\alpha_{m_1}}{\alpha_{m_2}}+1\right)\frac{L+a}{L}\tan\phi_3-\left(1+\frac{\alpha_{m_3}}{\alpha_{m_2}}\right)\frac{L+b}{L}\tan\phi_4\right\} \tag{A.11o}$$
$$+\frac{\left(L-a-b\right)\cos\theta_{G_2}}{J_2h}\left(\frac{-M_1}{\cos\phi_1}+\frac{M_2}{\cos\phi_2}-\frac{M_3}{\cos\phi_3}+\frac{M_4}{\cos\phi_4}\right)$$
$$-\frac{3\alpha_{m_1}}{\alpha_{m_2}}\frac{L-a}{L\left(L-a-b\right)}\cos\theta_{G_2}\left(\ddot V_{g_1}-h\sin\phi_1\dot\phi_1^2\right)$$
$$-\frac{3\alpha_{m_1}}{\alpha_{m_2}}\frac{L+a}{L\left(L-a-b\right)}\cos\theta_{G_2}\left(\ddot V_{g_3}-h\sin\phi_3\dot\phi_3^2\right)$$
$$-\frac{1}{L\left(L-a-b\right)\cos\theta_{G_2}}\left[-a\left(\ddot V_{g_1}-h\sin\phi_1\dot\phi_1^2\right)+b\left(\ddot V_{g_2}-h\sin\phi_2\dot\phi_2^2\right)\right.$$
$$\left.+\left(L+a\right)\left(\ddot V_{g_3}-h\sin\phi_3\dot\phi_3^2\right)-\left(L+b\right)\left(\ddot V_{g_4}-h\sin\phi_4\dot\phi_4^2\right)\right]-\tan\theta_{G_2}\dot\theta_{G_2}^2$$

$$c_{41}=0 \tag{A.11p}$$

$$c_{43} = 0 \tag{A.11q}$$

$$c_{42} = \left[\frac{3(L-b)}{L(L+b)}\cos\theta_{G_3} + \frac{1}{L\cos\theta_{G_3}}\right] h\cos\phi_2 \tag{A.11r}$$

$$c_{44} = \left[\frac{3}{L}\cos\theta_{G_3} - \frac{1}{L\cos\theta_{G_3}}\right] h\cos\phi_4 \tag{A.11s}$$

$$\begin{aligned} c_{45} = {} & \frac{K_{T_C}}{J_3}\Phi\left(\theta_{g_2} - \theta_{G_3}\right) + \frac{C_{T_C}}{J_3}\left(\dot\theta_{g_2} - \dot\theta_{G_3}\right) + \frac{K_{T_C}}{J_3}\Phi\left(\theta_{g_4} - \theta_{G_3}\right) + \frac{C_{T_C}}{J_3}\left(\dot\theta_{g_4} - \dot\theta_{G_3}\right) \\ & - 6\left[1 - \left(1 + \frac{\alpha_{m_2}}{\alpha_{m_3}}\right)\frac{b}{L}\right]\frac{g\cos\theta_{G_3}}{L+b}\tan\phi_2 + \frac{2M_2}{J_3 h\cos\phi_2}(L+b)\cos\theta_{G_3} \\ & - 6\left(1 + \frac{\alpha_{m_2}}{\alpha_{m_3}}\right)\frac{b}{L(L+b)}g\cos\theta_{G_3}\tan\phi_4 + \frac{2M_4}{J_3 h\cos\phi_4}b\cos\theta_{G_3} \\ & + \frac{3(L-b)}{L(L+b)}\cos\theta_{G_3}\left(\ddot V_{g_2} - h\sin\phi_2\dot\phi_2^2\right) + \frac{3}{L}\cos\theta_{G_3}\left(\ddot V_{g_4} - h\sin\phi_4\dot\phi_4^2\right) \\ & - \frac{1}{L\cos\theta_{G_3}}\left(\ddot V_{g_4} - \ddot V_{g_2} - h\sin\phi_4\dot\phi_4^2 + h\sin\phi_2\dot\phi_2^2\right) - \tan\theta_{G_3}\dot\theta_{G_3}^2 \end{aligned} \tag{A.11t}$$

For small deformations in a linear system and by neglecting the contributions of gravity, damping, input ground motion and high-order terms, Equations (A.8a)–(A.8d) can be written as

$$\begin{aligned} & \left[-m_1(L-a) + m_2 a\right]\frac{h}{2L}\ddot\phi_1 + \left[m_2 b - m_3(L-b)\right]\frac{h}{2L}\ddot\phi_2 - (m_1+m_2)\frac{L+a}{2L}h\ddot\phi_3 \\ & \qquad - (m_2+m_3)\frac{L+b}{2L}h\ddot\phi_4 - \frac{2K_\phi}{h}(\phi_1+\phi_2+\phi_3+\phi_4) = 0 \end{aligned} \tag{A.12a}$$

$$\begin{aligned} & \left[\frac{-m_1(L^2-a^2)}{4L} - \frac{J_1}{L}\right]h\ddot\phi_1 + \left[\frac{-m_1(L+a)^2}{4L} + \frac{J_1}{L}\right]h\ddot\phi_3 - \frac{2K_{T_C}h}{L}(\phi_1-\phi_3) - 2K_\phi\frac{L+a}{h}\phi_1 \\ & \qquad - 2K_\phi\frac{a}{h}\phi_3 = 0 \end{aligned} \tag{A.12b}$$

$$\begin{aligned} & \left[\frac{-m_1(L-a)(L-a-b)}{4L} + \frac{J_2 a}{L(L-a-b)}\right]h\ddot\phi_1 + \left[\frac{m_3(L-b)(L-a-b)}{4L}\right. \\ & \left. - \frac{J_2 b}{L(L-a-b)}\right]h\ddot\phi_2 + \left[\frac{-m_1(L+a)(L-a-b)}{4L} - \frac{J_2(L+a)}{L(L-a-b)}\right]h\ddot\phi_3 \\ & + \left[\frac{m_3(L+b)(L-a-b)}{4L} + \frac{J_2(L+b)}{L(L-a-b)}\right]h\ddot\phi_4 - \frac{K_\phi}{h}(L-a-b)(\phi_1-\phi_2+\phi_3-\phi_4) = 0 \end{aligned} \tag{A.12c}$$

$$\begin{aligned} & \left[\frac{m_3(L^2-b^2)}{4L} + \frac{J_3}{L}\right]h\ddot\phi_2 + \left[\frac{m_3(L+b)^2}{4L} - \frac{J_3}{L}\right]h\ddot\phi_4 - 2K_{T_C}\frac{h}{L}(\phi_4-\phi_2) + \frac{2K_\phi}{h}(L+b)\phi_2 \\ & \qquad + \frac{2K_\phi}{h}b\phi_4 = 0 \end{aligned} \tag{A.12d}$$

On assuming $m_1 = m_3$ and $a = b$, the Fourier transformation of these equations leads to

$$\left\{\left[\alpha_{m_1}(L-a)\frac{h}{2L}-\alpha_{m_2}\frac{ah}{2L}\right]\omega^2-\frac{2K_\phi}{mh}\right\}(\phi_1+\phi_2)+\left[\left(\alpha_{m_1}+\alpha_{m_2}\right)(L+a)\frac{h}{2L}\omega^2-\frac{2K_\phi}{mh}\right](\phi_3+\phi_4)=0 \tag{A.13a}$$

$$\left\{\frac{\left(4L^2+2La-2a^2\right)\alpha_{m_1}h\omega^2}{9L^3}-\frac{8}{3}\left[\frac{K_{T_c}h}{mL^3}+\frac{K_\phi(L+a)}{mL^2h}\right]\right\}\phi_1+\left[\frac{2}{9}\frac{(L+a)^2\alpha_{m_1}h\omega^2}{L^3}+\frac{8}{3}\left(\frac{K_{T_c}h}{mL^3}-\frac{K_\phi a}{mL^2h}\right)\right]\phi_3=0 \tag{A.13b}$$

$$\left\{\left[\frac{\alpha_{m_1}\left(L^2-3aL+2a^2\right)}{3L^3}-\frac{\alpha_{m_2}\left(aL-2a^2\right)}{9L^3}\right]h\omega^2-\frac{4}{3}\frac{K_\phi(L-2a)}{mL^2h}\right\}(\phi_1-\phi_2)+\left[\frac{\left(3\alpha_{m_1}+\alpha_{m_2}\right)\left(L^2-aL-2a^2\right)}{9L^3}h\omega^2-\frac{4}{3}\frac{K_\phi(L-2a)}{mL^2h}\right](\phi_3-\phi_4)=0 \tag{A.13c}$$

$$\left[\frac{-\left(4L^2+2aL-2a^2\right)}{9L^3}\alpha_{m_1}h\omega^2+\frac{8}{3}\frac{K_{T_C}h}{mL^3}+\frac{8}{3}\frac{K_\phi(L+a)}{mL^2h}\right]\phi_2-\left[\frac{2(L+a)^2}{9L^3}\alpha_{m_1}h\omega^2+\frac{8}{3}\frac{K_{T_C}h}{mL^3}-\frac{8}{3}\frac{K_\phi a}{mL^2h}\right]\phi_4=0 \tag{A.13d}$$

The above equations can be written in the matrix form as

$$\begin{bmatrix}c_{11}&c_{12}&c_{13}&c_{14}\\c_{21}&c_{22}&c_{23}&c_{24}\\c_{31}&c_{32}&c_{33}&c_{34}\\c_{41}&c_{42}&c_{43}&c_{44}\end{bmatrix}\begin{Bmatrix}\phi_1\\\phi_2\\\phi_3\\\phi_4\end{Bmatrix}=\begin{Bmatrix}0\\0\\0\\0\end{Bmatrix} \tag{A.14}$$

where,

$$c_{11}=c_{12}=\left[\alpha_{m_1}(L-a)\frac{h}{2L}-\alpha_{m_2}\frac{ah}{2L}\right]\omega^2-\frac{2K_\phi}{mh} \tag{A.15a}$$

$$c_{13}=c_{14}=\left(\alpha_{m_1}+\alpha_{m_2}\right)(L+a)\frac{h}{2L}\omega^2-\frac{2K_\phi}{mh} \tag{A.15b}$$

$$c_{21}=\frac{\left(4L^2+2La-2a^2\right)\alpha_{m_1}h\omega^2}{9L^3}-\frac{8}{3}\left[\frac{K_{T_c}h}{mL^3}+\frac{K_\phi(L+a)}{mL^2h}\right] \tag{A.15c}$$

$$c_{22}=c_{24}=0 \tag{A.15d}$$

$$c_{23}=\frac{2}{9}\frac{(L+a)^2\alpha_{m_1}h\omega^2}{L^3}+\frac{8}{3}\left(\frac{K_{T_c}h}{mL^3}-\frac{K_\phi a}{mL^2h}\right) \tag{A.15e}$$

$$c_{31}=-c_{32}=\left[\frac{\alpha_{m_1}\left(L^2-3aL+2a^2\right)}{3L^3}-\frac{\alpha_{m_2}\left(aL-2a^2\right)}{9L^3}\right]h\omega^2-\frac{4}{3}\frac{K_\phi(L-2a)}{mL^2h} \tag{A.15f}$$

$$c_{33} = -c_{34} = \frac{\left(3\alpha_{m_1} + \alpha_{m_2}\right)\left(L^2 - aL - 2a^2\right)}{9L^3} h\omega^2 - \frac{4}{3}\frac{K_\phi\left(L-2a\right)}{mL^2h} \tag{A.15g}$$

$$c_{41} = c_{43} = 0 \tag{A.15h}$$

$$c_{42} = -c_{21} \tag{A.15i}$$

$$c_{44} = -c_{23} \tag{A.15j}$$

For a nonzero solution of Equation (A.14) the determinant of the coefficient matrix $[C]$ should be zero. Therefore, we have

$$\left|[C]\right| = \begin{vmatrix} c_{11} & c_{12} & c_{13} & c_{14} \\ c_{21} & 0 & c_{23} & 0 \\ c_{31} & c_{32} & c_{33} & c_{34} \\ 0 & c_{42} & 0 & c_{44} \end{vmatrix} = 0 \quad \Rightarrow \quad \left(c_{23}c_{31} - c_{21}c_{33}\right)\left(c_{13}c_{21} - c_{11}c_{23}\right) = 0 \tag{A.16}$$

If, for example, $a = b = L/5$, then by solving Equation (A.16), one can find the natural frequencies of the bridge as follows:

$$\begin{aligned}\left|[C]\right| = \Bigg(& 0.013654\frac{h^2}{L^2}\omega^4 - 0.462217\frac{K_{T_c}h^2}{mL^4}\omega^2 - 0.37689\frac{K_\phi}{mL^2}\omega^2 + 4.2667\frac{K_\phi K_{T_c}}{m^2L^4} \\ & + 2.1336\frac{K_\phi^2}{m^2L^2h^2}\Bigg)\Bigg(-0.0512\frac{h^2}{L}\omega^4 + \frac{4}{3}\frac{K_{T_c}h^2}{mL^3}\omega^2 + 1.2053\frac{K_\phi}{mL}\omega^2 - \frac{32}{3}\frac{K_\phi K_{T_c}}{m^2L^3} \\ & - 5.333\frac{K_\phi^2}{m^2Lh^2}\Bigg) = 0\end{aligned} \tag{A.17a}$$

$$K_{T_c} = 0 \quad \Rightarrow \quad \begin{cases} \omega_1^2 = 5.9066\dfrac{K_\phi}{mh^2}, & \omega_2^2 = 7.95\dfrac{K_\phi}{mh^2} \\ \omega_3^2 = 17.6344\dfrac{K_\phi}{mh^2}, & \omega_4^2 = 19.653\dfrac{K_\phi}{mh^2} \end{cases} \tag{A.17b}$$

$$\begin{cases} K_{T_c} = 0.5K_\phi \\ \dfrac{L}{h} = 5 \end{cases} \quad \Rightarrow \quad \begin{cases} \omega_1^2 = 6.0\dfrac{K_\phi}{mh^2}, & \omega_2^2 = 8.0217\dfrac{K_\phi}{mh^2} \\ \omega_3^2 = 18.065\dfrac{K_\phi}{mh^2}, & \omega_4^2 = 20.259\dfrac{K_\phi}{mh^2} \end{cases} \tag{A.17c}$$

$$\begin{cases} K_{T_c} = K_\phi \\ \dfrac{L}{h} = 5 \end{cases} \quad \Rightarrow \quad \begin{cases} \omega_1^2 = 6.08\dfrac{K_\phi}{mh^2}, & \omega_2^2 = 8.0854\dfrac{K_\phi}{mh^2} \\ \omega_3^2 = 18.5\dfrac{K_\phi}{mh^2}, & \omega_4^2 = 20.8723\dfrac{K_\phi}{mh^2} \end{cases} \tag{A.17d}$$

$$\begin{cases} K_{T_c} = 1.5K_\phi \\ \dfrac{L}{h} = 5 \end{cases} \quad \Rightarrow \quad \begin{cases} \omega_1^2 = 6.16\dfrac{K_\phi}{mh^2}, & \omega_2^2 = 8.1425\dfrac{K_\phi}{mh^2} \\ \omega_3^2 = 18.95\dfrac{K_\phi}{mh^2}, & \omega_4^2 = 21.4935\dfrac{K_\phi}{mh^2} \end{cases} \tag{A.17e}$$

From these equations it is seen that the effect of torsional stiffness of piers on the natural frequencies of the bridge is small. By neglecting the torsional stiffness and damping of piers (i.e., K_{T_c} = 0, C_{T_c} = 0), one can determine the rotational damping coefficients of the system for the prescribed fraction of critical damping. The mass, stiffness, and damping matrices of the bridge thus become

$$[M]=mh\begin{bmatrix}0.11467 & 0.00133 & 0.032 & -0.008\\ 0.00133 & 0.11467 & -0.008 & 0.032\\ 0.032 & -0.008 & 0.288 & 0.048\\ -0.008 & 0.032 & 0.048 & 0.288\end{bmatrix} \tag{A.18a}$$

$$[K]=\begin{bmatrix}\frac{2K_\phi}{h} & 0 & 0 & 0\\ 0 & \frac{2K_\phi}{h} & 0 & 0\\ 0 & 0 & \frac{2K_\phi}{h} & 0\\ 0 & 0 & 0 & \frac{2K_\phi}{h}\end{bmatrix} \tag{A.18b}$$

$$[C]=\begin{bmatrix}\frac{2C_\phi}{h} & 0 & 0 & 0\\ 0 & \frac{2C_\phi}{h} & 0 & 0\\ 0 & 0 & \frac{2C_\phi}{h} & 0\\ 0 & 0 & 0 & \frac{2C_\phi}{h}\end{bmatrix} \tag{A.18c}$$

The natural frequencies and symmetric and asymmetric mode shapes of the system are then obtained as (see Figure A.4)

$$\left|[K]-\omega^2[M]\right|=0 \;\Rightarrow\; \begin{cases}\omega_1^2=\dfrac{5.9066K_\phi}{mh^2},\ \omega_2^2=\dfrac{7.954K_\phi}{mh^2},\ \omega_3^2=\dfrac{17.635K_\phi}{mh^2},\ \omega_4^2=\dfrac{19.65K_\phi}{mh^2}\\ [\Phi]=\begin{bmatrix}1 & 1 & 1 & 1\\ 1 & -1 & 1 & -1\\ 9.271 & 3.448 & -0.1078 & -0.289\\ 9.271 & -3.448 & -0.1078 & 0.289\end{bmatrix}\end{cases} \tag{A.19}$$

In modal space the mass, stiffness, and damping matrices of the bridge are

$$[M_n]=[\Phi]^T[M][\Phi]=mh\begin{bmatrix}58.9 & 0 & 0 & 0\\ 0 & 6.485 & 0 & 0\\ 0 & 0 & 0.2295 & 0\\ 0 & 0 & 0 & 0.2206\end{bmatrix} \tag{A.20a}$$

$$[K_n]=[\Phi]^T[K][\Phi]=\frac{K_\phi}{h}\begin{bmatrix}347.81 & 0 & 0 & 0\\ 0 & 51.56 & 0 & 0\\ 0 & 0 & 4.05 & 0\\ 0 & 0 & 0 & 4.334\end{bmatrix} \tag{A.20b}$$

$$[C_n] = [\Phi]^T [C][\Phi] = \frac{C_\phi}{h} \begin{bmatrix} 347.81 & 0 & 0 & 0 \\ 0 & 51.56 & 0 & 0 \\ 0 & 0 & 4.05 & 0 \\ 0 & 0 & 0 & 4.334 \end{bmatrix} \tag{A.20c}$$

The damping ratio of the *i*th mode is

$$\xi_i = \frac{C_i}{2M_i\omega_i} \tag{A.21}$$

and, thus for the first mode, we have

$$\xi_1 = 0.02 \quad \Rightarrow \quad \frac{C_\phi}{mh^2} = 0.00677\omega_1 \tag{A.22}$$

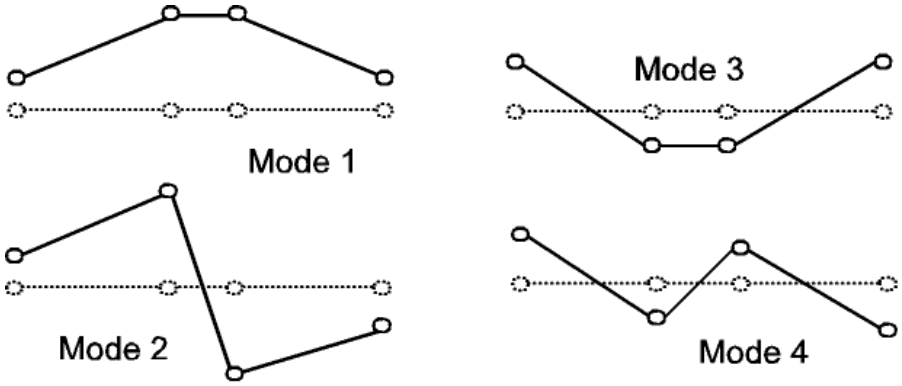

Fig. A.4 Symmetric and antisymmetric mode shapes of the bridge

APPENDIX II: NEAR-FAULT GROUND MOTION

It is difficult to predict strong ground motions near faults due to the irregular distribution of slip (Mavroeidis et al., 2004; Trifunac, 1974; Trifunac and Udwadia, 1974), non-uniform distribution of geologic rigidities surrounding the fault, irregular distribution of stress on the fault and complex nonlinear processes that accompany the fault motions during earthquakes. Thus, it is hard to predict the detailed nature of a near-fault ground motion and of the associated strong-motion pulses in time. In this study, a simplified approach is adopted and these motions are modeled by smooth functions, which have correct average amplitudes and durations and which have been calibrated against the observed fault slips and the recorded strong motions in terms of their peak amplitudes in time and their spectral content (Trifunac, 1993a, 1993b).

Figure A.5 shows schematically a fault and two simple motions, d_N and d_F, which describe the monotonic growth of the displacement toward the permanent static offset and a pulse, which is usually perpendicular to the fault surface and is associated with the failure of a nearby asperity or the passage of dislocation under or past the observation point (Haskell, 1969). In this paper the motions d_N and d_F represent the fault-parallel and fault-normal motions, respectively, of any fault system with shear type dislocation. For the fault-normal pulse, one can choose (see Figure A.5)

$$d_F(t) = A_F t e^{-\alpha_F t} \tag{A.23}$$

The values of A_F and α_F versus earthquake magnitudes are shown in Table A.1 (Trifunac, 1993b). For the fault-parallel permanent displacement, one can consider (see Figure A.5)

$$d_N(t) = \frac{A_N}{2}\left(1 - e^{-t/\tau_N}\right) \tag{A.24}$$

The values of A_N and τ_N versus earthquake magnitudes are shown in Table A.2. Because the strong-motion data are abundant only up to about M = 6.5, we place the values of α_F, A_F, τ_N, and A_N for M = 7 (in Tables A.1 and A.2) in parentheses to emphasize that those are based on extrapolation.

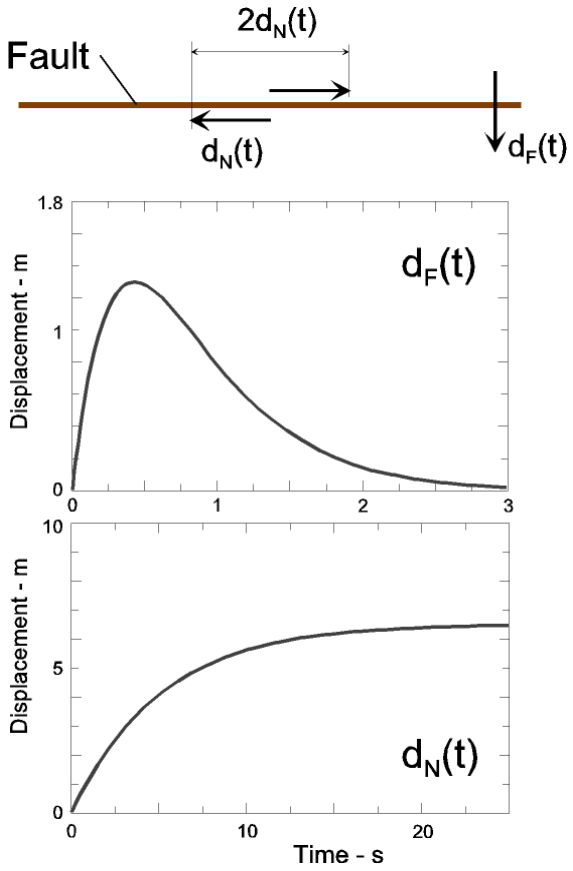

Fig. A.5 Fault-parallel displacement $d_N(t)$ and fault-normal displacement $d_F(t)$ for magnitude $M = 7$

The amplitudes of d_F and d_N have been studied in numerous regression analyses of recorded peak displacements at various distances from the faults and in terms of the observed surface expressions of the fault slips. The latter are traditionally presented as average dislocation amplitudes, $\overline{u}$, and are related to d_N as $\overline{u} = 2d_N$ (see Figure A.5). An important property of the d_F and d_N functions, as used in this study, is their initial velocity. It can be shown that $\dot{d}_F \sim \sigma\beta/\mu$, where σ is the effective stress (which is approximately same as the stress drop) on the fault surface (Trifunac, 1993b, 1998), β is the velocity of shear waves in the fault zone, and μ is the rigidity of rocks surrounding the fault. Further, it can be shown that $\dot{d}_N = 0.5C_0\sigma\beta/\mu$ at t = 0, where the typical values of C_0 are 0.6, 0.65, 1.00, 1.52, and 1.52 for M = 4, 5, 6, 7, and 8 (Trifunac, 1993b, 1998). The largest peak velocity observed so far, at 5–10 km above the fault, is about 200 cm/s. For example, 170 cm/s was recorded during the Northridge, California earthquake of 1994 (Trifunac et al., 1998). Because there are no strong-motion measurements of peak ground velocity at the fault surface, the peak velocities $\dot{d}_F$ and $\dot{d}_N$ can be evaluated only indirectly in terms of σ. The accuracy of the stress estimates depends upon the assumptions and methods used in the interpretation of recorded strong-motion records, and it is typically about one order of magnitude. Therefore, by solving the above equations for σ, one can use $\sigma \sim 2\mu\dot{d}_N/\beta C_0$ and $\sigma \sim \mu\dot{d}_F/\beta$ to check their consistency with the other published estimates of σ (Trifunac, 2009).

Table A.1: Characteristics of Fault-Normal Pulse (Trifunac, 1993b)

M (magnitude)	α_F (1/s)	A_F (cm/s)	$d_{F,\max}$ (cm)	$\dot{d}_{F,\max}$ (cm/s)
4	14.04	56.48	1.48	56.48
5	7.90	151.61	7.06	151.61
6	4.44	546.97	45.32	546.97
7	(2.50)	(860.34)	(126.6)	(860.34)

Table A.2: Characteristics of Fault-Parallel Displacement (Trifunac, 1993b)

M (magnitude)	τ_N (s)	A_N (cm)	$d_{N,\max}$ (cm)	$\dot{d}_{N,\max}$ (cm/s)
4	0.55	4.9	2.45	4.45
5	1.2	29.2	14.6	12.17
6	1.8	245.5	122.75	68.19
7	(3.0)	(1288.0)	(644.0)	(214.7)

REFERENCES

1. Bogdanoff, J.L., Goldberg, J.E. and Schiff, A.J. (1965). “The Effect of Ground Transmission Time on the Response of Long Structures”, Bulletin of the Seismological Society of America, Vol. 55, No. 3, pp. 627–640.
2. Chouw, N. and Hao, H. (2003). “Effect of Simultaneous Spatial Near-Source Ground Excitation and Soil on the Pounding Response of Bridge Girders”, Journal of Applied Mechanics, JSCE, Vol. 6, pp. 779–788.
3. Chouw, N. and Hao, H. (2004). “Investigation of Soil-Structure Interaction and Near-Source Ground Motion Spatial Variation Effect on Pounding of Bridge Girders”, Proceedings of the 11th International Conference on Soil Dynamics and Earthquake Engineering and the Third International Conference on Earthquake Geotechnical Engineering, Berkeley, U.S.A., Vol. 2, pp. 726–733.
4. Chouw, N. and Hao, H. (2005). “Study of SSI and Non-uniform Ground Motion Effect on Pounding between Bridge Girders”, Soil Dynamics and Earthquake Engineering, Vol. 25, No. 7, pp. 717–728.
5. Dicleli, M. (2008). “Performance of Seismic-Isolated Bridges with and without Elastic-Gap Devices in Near-Fault Zones”, Earthquake Engineering & Structural Dynamics, Vol. 37, No. 6, pp. 935–954.
6. Fenves, G.L. and Ellery, M. (1998). “Behavior and Failure Analysis of a Multiple-Frame Highway Bridge in the 1994 Northridge Earthquake”, Report PEER 98/08, University of California, Berkeley, U.S.A.
7. Goel, R.K. and Chopra, A.K. (2008). “Role of Shear Keys in Seismic Behavior of Bridges Crossing Fault-Rupture Zones”, Journal of Bridge Engineering, ASCE, Vol. 13, No. 4, pp. 398–408.
8. Hall, J.F., Heaton, T.H., Halling, M.W. and Wald, D.J. (1995). “Near Source Ground Motion and Its Effects on Flexible Buildings”, Earthquake Spectra, Vol. 11, No. 4, pp. 569–605.
9. Hao, H. (1991). “Response of Multiply Supported Rigid Plate to Spatially Correlated Seismic Excitation”, Earthquake Engineering & Structural Dynamics, Vol. 20, No. 9, pp. 821–838.
10. Hao, H. (1998). “A Parametric Study of the Required Seating Length for Bridge Decks during Earthquake”, Earthquake Engineering & Structural Dynamics, Vol. 27, No. 1, pp. 91–103.
11. Harichandran, R.S. and Wang, W. (1988). “Response of Simple Beam to Spatially Varying Earthquake Excitation”, Journal of Engineering Mechanics, ASCE, Vol. 114, No. 9, pp. 1526–1541.
12. Harichandran, R.S. and Wang, W. (1990). “Response of Intermediate Two-Span Beam to Spatially Varying Seismic Excitation”, Earthquake Engineering & Structural Dynamics, Vol. 19, No. 2, pp. 173–187.
13. Haskell, N.A. (1969). “Elastic Displacements in the Near Field of a Propagating Fault”, Bulletin of the Seismological Society of America, Vol. 59, No. 2, pp. 865–908.

14. Hyun, C.H., Yun, C.B. and Lee, D.G. (1992). "Nonstationary Response Analysis of Suspension Bridges for Multiple Support Excitations", Probabilistic Engineering Mechanics, Vol. 7, No. 1, pp. 27–35.
15. Jalali, R.S. and Trifunac, M.D. (2007). "Strength-Reduction Factors for Structures Subjected to Differential Near-Source Ground Motions", ISET Journal of Earthquake Technology, Vol. 44, No. 1, pp. 285–304.
16. Jalali, R.S. and Trifunac, M.D. (2008). "A Note on Strength Reduction Factors for Design of Structures near Earthquake Faults", Soil Dynamics and Earthquake Engineering, Vol. 28, No. 3, pp. 212–222.
17. Jalali, R.S. and Trifunac, M.D. (2009). "Response Spectra for Near-Source, Differential and Rotational Strong Ground Motion", Bulletin of the Seismological Society of America, Vol. 99, No. 2B, pp. 1404–1415.
18. Jalali, R.S. and Trifunac, M.D. (2011). "A Note on the Wave-Passage Effects in Out-of-Plane Response of Long Structures to Strong Earthquake Pulses", Soil Dynamics and Earthquake Engineering, Vol. 31, No. 4, pp. 640–647.
19. Jalali, R.S., Trifunac, M.D., Amiri, G.G. and Zahedi, M. (2007). "Wave-Passage Effects on Strength-Reduction Factors for Design of Structures near Earthquake Faults", Soil Dynamics and Earthquake Engineering, Vol. 27, No. 8, pp. 703–711.
20. Jalali, R.S., Jokandan, M.B. and Trifunac, M.D. (2012). "Earthquake Response of a Three-Span, Simply Supported Bridge to Near-Field Pulse and Permanent-Displacement Step", Soil Dynamics and Earthquake Engineering, Vol. 43, pp. 380–397.
21. Jonsson, M.H., Bessason, B. and Haflidason, E. (2010). "Earthquake Response of a Base-Isolated Bridge Subjected to Strong Near-Fault Ground Motion", Soil Dynamics and Earthquake Engineering, Vol. 30, No. 6, pp. 447–455.
22. Kashefi, I. and Trifunac, M.D. (1986). "Investigation of Earthquake Response of Simple Bridge Structures", Report CE 86-02, University of Southern California, Los Angeles, U.S.A.
23. Kojić, S. and Trifunac, M.D. (1988). "Earthquake Response of Arch Dams to Non-uniform Canyon Motion", Report CE 88-03, University of Southern California, Los Angeles, U.S.A.
24. Kojić, S. and Trifunac, M.D. (1991a). "Earthquake Stresses in Arch Dams: I—Theory and Anti-plane Excitation", Journal of Engineering Mechanics, ASCE, Vol. 117, No. 3, pp. 532–552.
25. Kojić, S.B. and Trifunac, M.D. (1991b). "Earthquake Stresses in Arch Dams: II—Excitation by SV-, P- and Rayleigh Waves", Journal of Engineering Mechanics, ASCE, Vol. 117, No. 3, pp. 553–574.
26. Mavroeidis, G.P., Dong, G. and Papageorgiou, A.S. (2004). "Near-Fault Ground Motions, and the Response of Elastic and Inelastic Single-Degree-of-Freedom (SDOF) Systems", Earthquake Engineering & Structural Dynamics, Vol. 33, No. 9, pp. 1023–1049.
27. Mylonakis, G. and Reinhorn, A.M. (2001). "Yielding Oscillator under Triangular Ground Acceleration Pulse", Journal of Earthquake Engineering, Vol. 5, No. 2, pp. 225–251.
28. Okubo, T., Arakawa, T. and Kawashima, K. (1983). "Preliminary Analysis of Finite Ground Strains Induced during Earthquakes and Effect of Spatial Ground Motions on Structural Response" in "Earthquake Behavior and Safety of Oil and Gas Storage Facilities, Buried Pipelines and Equipment (edited by T. Ariman)", Report PVP-Vol. 77, American Society of Mechanical Engineers, New York, U.S.A.
29. Perotti, F. (1990). "Structural Response to Non-stationary Multiple Support Random Excitation", Earthquake Engineering & Structural Dynamics, Vol. 19, No. 4, pp. 513–527.
30. Todorovska, M.I. and Lee, V.W. (1989). "Seismic Waves in Buildings with Shear Walls or Central Core", Journal of Engineering Mechanics, ASCE, Vol. 115, No. 12, pp. 2669–2686.
31. Todorovska, M.I. and Trifunac, M.D. (1989). "Anti-plane Earthquake Waves in Long Structures", Journal of Engineering Mechanics, ASCE, Vol. 115, No. 12, pp. 2687–2708.
32. Todorovska, M.I. and Trifunac, M.D. (1990a). "A Note on the Propagation of Earthquake Waves in Buildings with Soft First Floor", Journal of Engineering Mechanics, ASCE, Vol. 116, No. 4, pp. 892–900.

33. Todorovska, M.I. and Trifunac, M.D. (1990b). "A Note on Excitation of Long Structures by Ground Waves", Journal of Engineering Mechanics, ASCE, Vol. 116, No. 4, pp. 952–964.
34. Todorovska, M.I. and Trifunac, M.D. (1997). "Amplitudes, Polarity and Time of Peaks of Strong Ground Motion during the 1994 Northridge, California Earthquake", Soil Dynamics and Earthquake Engineering, Vol. 16, No. 4, pp. 235–258.
35. Todorovska, M.I., Trifunac, M.D., Lee, V.W. and Orbović, N. (2013). "Synthetic Earthquake Ground Motions on an Array", Soil Dynamics and Earthquake Engineering, Vol. 48, pp. 234–251.
36. Trifunac, M.D. (1974). "A Three-Dimensional Dislocation Model for the San Fernando, California, Earthquake of February 9, 1971", Bulletin of the Seismological Society of America, Vol. 64, No. 1, pp. 149–172.
37. Trifunac, M.D. (1993a). "Long Period Fourier Amplitude Spectra of Strong Motion Acceleration", Soil Dynamics and Earthquake Engineering", Vol. 12, No. 6, pp. 363–382.
38. Trifunac, M.D. (1993b). "Broad Band Extension of Fourier Amplitude Spectra of Strong Motion Acceleration", Report CE 93-01, University of Southern California, Los Angeles, U.S.A.
39. Trifunac, M.D. (1997). "Relative Earthquake Motion of Building Foundations", Journal of Structural Engineering, ASCE, Vol. 123, No. 4, pp. 414–422.
40. Trifunac, M.D. (1998). "Stresses and Intermediate Frequencies of Strong Motion Acceleration", Geofizika, Vol. 14, No. 1, pp. 1–27.
41. Trifunac, M.D. (2009). "The Role of Strong Motion Rotations in the Response of Structures near Earthquake Faults", Soil Dynamics and Earthquake Engineering, Vol. 29, No. 2, pp. 382–393.
42. Trifunac, M.D. and Gicev, V. (2006). "Response Spectra for Differential Motion of Columns Paper II: Out-of-Plane Response", Soil Dynamics and Earthquake Engineering, Vol. 26, No. 12, pp. 1149–1160.
43. Trifunac, M.D. and Todorovska, M.I. (1994). "Broad Band Extension of Pseudo Relative Velocity Spectra of Strong Motion", Report CE 94-02, University of Southern California, Los Angeles, U.S.A.
44. Trifunac, M.D. and Todorovska, M.I. (1996). "Nonlinear Soil Response—1994 Northridge, California Earthquake", Journal of Geotechnical Engineering, ASCE, Vol. 122, No. 9, pp. 725–735.
45. Trifunac, M.D. and Todorovska, M.I. (1997a). "Response Spectra and Differential Motion of Columns", Earthquake Engineering & Structural Dynamics, Vol. 26, No. 2, pp. 251–268.
46. Trifunac, M.D. and Todorovska, M.I. (1997b). "Northridge, California, Earthquake of 1994: Density of Red-Tagged Buildings versus Peak Horizontal Velocity and Intensity of Shaking", Soil Dynamics and Earthquake Engineering, Vol. 16, No. 3, pp. 209–222.
47. Trifunac, M.D. and Todorovska, M.I. (1997c). "Northridge, California, Earthquake of 1994: Density of Pipe Breaks and Surface Strains", Soil Dynamics and Earthquake Engineering, Vol. 16, No. 3, pp. 193–207.
48. Trifunac, M.D. and Udwadia, F.E. (1974). "Parkfield, California, Earthquake of June 27, 1966: A Three-Dimensional Moving Dislocation", Bulletin of the Seismological Society of America, Vol. 64, No. 3, pp. 511–533.
49. Trifunac, M.D., Todorovska, M.I. and Ivanović, S.S. (1996). "Peak Velocities and Peak Surface Strains during Northridge, California, Earthquake of 17 January 1994", Soil Dynamics and Earthquake Engineering, Vol. 15, No. 5, pp. 301–310.
50. Trifunac, M.D., Todorovska, M.I. and Lee, V.W. (1998). "The Rinaldi Strong Motion Accelerogram of the Northridge, California, Earthquake of 17 January 1994", Earthquake Spectra, Vol. 14, No. 1, pp. 225–239.
51. Zanardo, G., Hao, H. and Modena, C. (2002). "Seismic Response of Multi-span Simply Supported Bridges to a Spatially Varying Earthquake Ground Motion", Earthquake Engineering & Structural Dynamics, Vol. 31, No. 6, pp. 1325–1345.
52. Zembaty, Z. and Krenk, S. (1993). "Spatial Seismic Excitations and Response Spectra", Journal of Engineering Mechanics, ASCE, Vol. 119, No. 12, pp. 2449–2460.
53. Zembaty, Z. and Krenk, S. (1994). "Response Spectra of Spatial Seismic Ground Motion", Proceedings of the 10th European Conference on Earthquake Engineering, Vienna, Austria, Vol. 2, pp. 1271–1275.

54. Zerva, A. (1991). “Effect of Spatial Variability and Propagation of Seismic Ground Motions on the Response of Multiply Supported Structures”, Probabilistic Engineering Mechanics, Vol. 6, No. 3-4, pp. 212–221.